M.O. 715

METEOROLOGICAL OFFICE

Scientific Paper No. 13

Three-Parameter Numerical Forecasts at Dunstable–a Study of the Error Fields

by C. E. WALLINGTON, M.Sc.

LONDON: HER MAJESTY'S STATIONERY OFFICE

PRICE 3s. 6d. NET

M.O. 715

METEOROLOGICAL OFFICE

Scientific Paper No. 13

Three-Parameter Numerical Forecasts at Dunstable—a Study of the Error Fields

by C. E. WALLINGTON, M.Sc.

LONDON
HER MAJESTY'S STATIONERY OFFICE
1962

U.D.C.: 551·509·313:
551·509·59

Contents

Three-Parameter Numerical Forecasts at Dunstable—A Study of the Error Fields

by C. E. Wallington, M.Sc.

INTRODUCTION

Early in 1960 a three-parameter numerical prediction model was formulated at Dunstable for use with the electronic computer, "Meteor", and as soon as the computing programme was completed the model was subjected to a four-month test. On almost every week-day in the period 29 February to 2 June 1960, 24- and 30-hour forecasts were made from the current midnight data. The initial data for each forecast comprised 1000 mb, 500 mb, and 200 mb contour heights for a network of 480 grid points covering the area shown in Figure 1, the distance between adjacent grid points ranging from about 130 to 170 nautical miles. The end product of the computations comprised forecast charts of the three contour fields already mentioned, together with the intervening thickness fields and fields of two computed vertical motion parameters. In view of the expedient, but generally incorrect, assumption that all contour heights at the boundary of the computing area would not change during the period of the forecast, hopes for satisfactory forecasts were limited to an inner "verification" area—a rectangular network of 192 grid points which covers approximately the same area as the routine forecast charts prepared at the Central Forecasting Office (C.F.O.) by conventional qualitative methods. This verification area is outlined in Figure 1.

After the forecasts had been completed a number of verification indices such as root mean square contour height errors and correlation coefficient between forecast and actual 24-hour changes in the verification area were computed for both the numerical and the C.F.O. forecasts. The same indices were also computed for "persistence" forecasts obtained by taking the initial contour fields as artificial 24-hour forecasts. The primary purpose of this paper is to provide a summary of the verification computations as a means of passing on the experience of numerical forecasting accrued during the four-month test to forecasters who are now being supplied with this three-parameter type of numerical forecast.

THE THREE-PARAMETER MODEL

The full details of the numerical model used are elaborated in a paper by Bushby and Whitelam[1], but before studying the nature of the forecasting errors we should note some relevant features of the model, namely:

(*i*) In each of the layers 1000–600 mb and 600–200 mb the thermal wind is assumed to be constant in direction in any vertical column and the thermal wind speed is assumed to be proportional to the pressure difference through any part of the column.

(*ii*) The vertical motion profile comprises two parabolae; one for the 1000–600 mb layer, the other for the 600–200 mb region. These parabolae have zero values at the 200 and 1000 mb levels and are continuous in both magnitude and direction at the 600 mb level.

(*iii*) The nature of the equations is such that, at the 600 mb level, the model behaves almost like a barotropic model.

(*iv*) The basic equations for the model are derived from the vorticity equations at 200 mb and 1000 mb but, for convenience, the principal working fields are the 600 mb contours

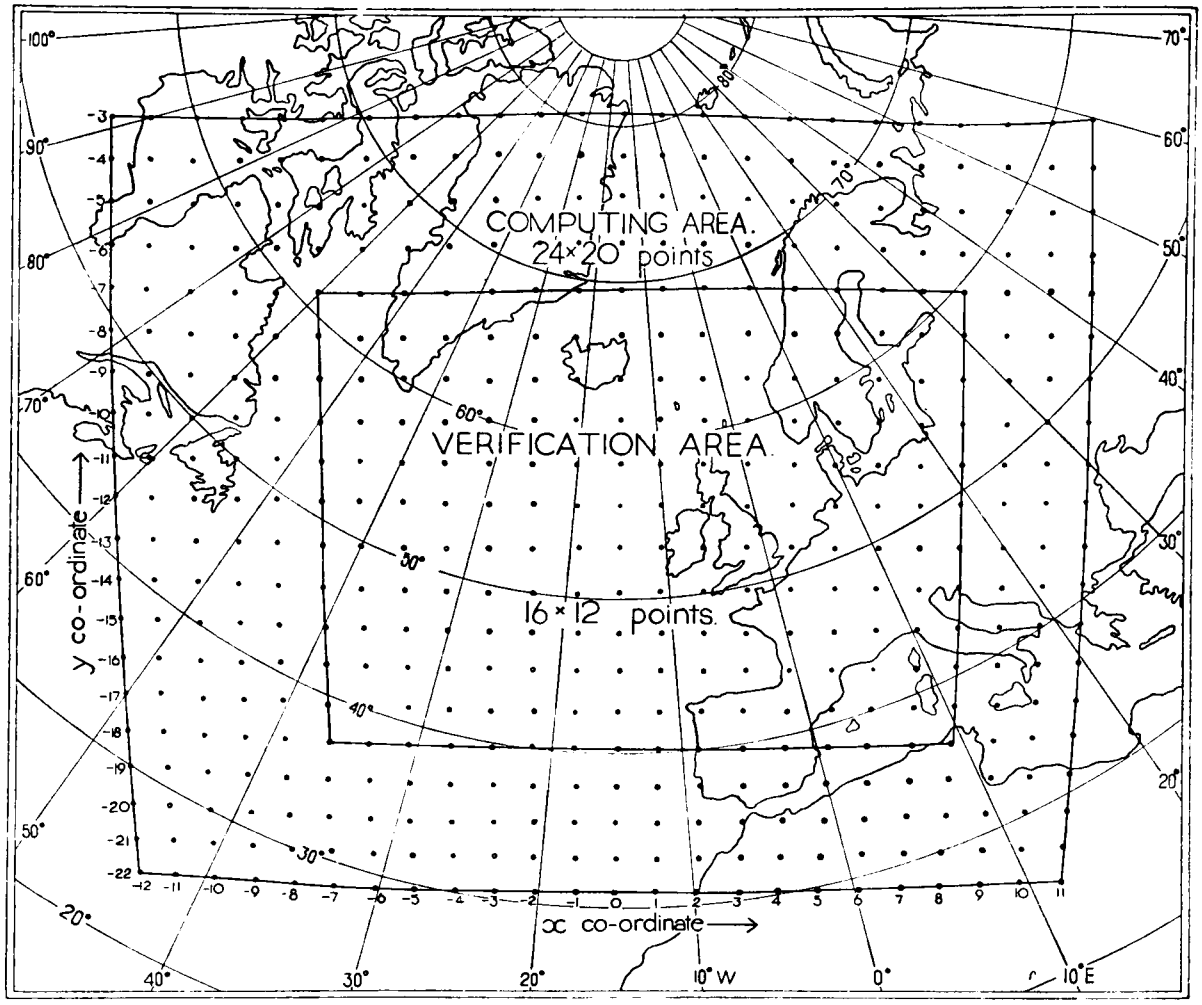

FIGURE 1. Computing grid for numerical forecasting experiment
The grid points form a square network on a stereographic projection from the South Pole on to a plane perpendicular to the earth's axis.
Grid length = 88.1412 (1 + sin ϕ) nautical miles where ϕ = latitude
= 176 nautical miles (325 km) at North Pole
= 164 nautical miles (303 km) at 60°N
= 132 nautical miles (244 km) at 30°N

and the adjoining thickness fields. The forecast mean-sea-level pressures and the 200 mb contours can be regarded as eventual by-products of the predicted mid-level and thickness forecasts. The 500 mb forecast is also a by-product to some extent but it is usually very similar to the 600 mb predictions.

(*v*) Terms expressing the vertical advection of vorticity and the twisting of vorticity axes from horizontal to vertical directions have been omitted from the model. These terms are often small but are likely to be important in active frontal regions.

(*vi*) The temperature lapse rates for the model are assumed to be 42°C per 1000 mb and 51°C per 1000 mb everywhere for the 1000–600 mb and 600–200 mb layers respectively.

(*vii*) The effect of heating over relatively warm sea is included in the model. Whenever the

1000–600 mb thickness in metres is less than 12·97 (T+282·5), where T°F is the monthly mean sea surface temperature, this thickness is increased at a statistically determined rate.[2]

(*viii*) The effects of topography and friction are ignored in the model.

(*ix*) The numerical forecasts using this model were made using $\frac{3}{4}$-hour time steps. This time step was sufficiently short to prevent erratic distortion of the contour fields due to computational instability in most, but not all, of the 24- and 30- hour forecasts prepared during the four-month test.

(*x*) The contour height changes at the two outer rows of grid points in the computing area are assumed to be zero during each forecast.

(*xi*) In the model, geostrophic winds measured over one grid length are used to compute vorticities, while contour gradients over two grid lengths are used to obtain wind speeds for advection.

(*xii*) The tropopause is ignored.

PRINCIPAL CAUSES OF THE FORECASTING ERRORS

Study of the numerical forecasts revealed two principal causes of error in the 24-hour forecasts, namely:

(*i*) The incorrect assumption of no change at and adjacent to the computing boundary.

(*ii*) Spurious anticyclogenesis at the 500 mb level.

Obviously the boundary assumption does not allow pressure systems to enter or leave the computing area, and it is not uncommon for the ensuing errors to spread into the verification area during a 24-hour period. When the excluded or trapped systems take the form of easily recognizable depressions or anticyclones on the initial charts, then this boundary effect can be easily anticipated, but when the changes in the pressure system take the form of less distinctive variations in vorticity due to wind shear the subsequent boundary effects are difficult to assess.

The effect of spurious anticyclogenesis in the two-parameter Sawyer–Bushby model has been discussed in some detail by Knighting, Corby, Bushby and Wallington.[3] Briefly, the effect is that the numerical prediction models of the type under discussion tend to overemphasize the development of high pressure systems, especially in broad airstreams from the south. Such spurious development often leads to excessive strengthening of the flow from the south, and, should there be a tongue of warm air in this region, the tongue is advected too far north. The consequence of this excessive advection of warm air is that low pressure systems to the north-west or north-north-west of the anticyclone are much too deep in the resultant M.S.L. pressure forecasts. Thus spurious anticyclogenesis at the mid-level leads to both spurious anticyclogenesis and cyclogenesis in the M.S.L. forecast, with excessively strong pressure gradients between the high and low systems. The correspondingly excessive advection in the upper thickness pattern, however, tends to weaken the 200 mb contour gradient very slightly, although this weakening is usually swamped by the mid-level tightening especially in the southern half of the verification area.

Boundary effects and spurious anticyclogenesis coupled with the excessive advection of the thickness pattern appear to be two major causes of errors in the model tested. Errors due to the neglect of topography in the model were suspected on several occasions but the topographical errors so far investigated have been mixed in indeterminate proportions with boundary effects and spurious anticyclogenesis.

PREVAILING SYNOPTIC SITUATIONS

Before considering the forecasting errors in detail it is advisable to note the principal features of the synoptic situations during the experimental period from 29 February to 2 June 1960. As illustrated in Figures 2 (*a*)–(*c*), the means of the M.S.L. pressure and upper level contour charts for the 55 24-hour periods used in the experiments revealed a low pressure system just south-east of Greenland with a broad diffluent flow from the west at high levels. Although many of the synoptic situations included very mobile systems with depression centres over the southern and eastern regions of the chart, several weeks of the experimental period were noted for the tendency of low pressure systems to move slowly from just south of Greenland towards the north-east, leaving much of the synoptic situation farther south-east almost unchanged. In fact many a 24-hour forecast was subjectively described as a "good forecast in a slowly changing situation". Thus these synoptic situations in the period were on average slightly less mobile than usual for the spring and early summer, and the error fields to be described must be considered in the light of the mean situation and the root mean square 24-hour changes which will be presented in the relevant sections to follow.

AVERAGE AND MAXIMUM ERRORS

During the four-month period of the experiment 55 24-hour forecasts were computed. Verification indices, such as the root mean square contour height error taken over the 192 grid points in the verification area, were computed not only for the numerical forecasts but also for the corresponding forecasts prepared by the C.F.O. forecasters and for "persistence"

TABLE I

(*a*) *Root mean square height errors in metres*

	Numerical forecasts	C.F.O. forecasts	Persistence
1000 mb	55	45	53
500–1000 mb	49	47	59
500 mb	57	61	76
200–500 mb	45	47	48
200 mb	69	71	91

(*b*) *Root mean square vector wind errors in knots*

	Numerical forecasts	C.F.O. forecasts	Persistence
1000 mb	21	18	20
500–1000 mb	27	22	26
500 mb	24	23	29
200–500 mb	25	20	21
200 mb	28	25	32

(*c*) *Correlation coefficient between forecast and actual contour height changes over the 24-hour period*

	Numerical forecasts	C.F.O. forecasts
1000 mb	0.56	0.61
500–1000 mb	0.65	0.63
500 mb	0.69	0.65
200–500 mb	0.54	0.49
200 mb	0.67	0.63

forecasts obtained by predicting zero changes for the 24-hour period. Table I shows the root mean square contour height (or thickness) errors, the root mean square vector wind

errors and the mean correlation coefficients between forecast and actual contour height changes computed for each forecast field.

On this statistical basis, the success of the numerical forecasting system applied to thickness and upper level charts was comparable with that attained by conventional methods. At the 1000 mb level, however, the numerical forecasting success was often marred by the effects of spurious anticyclogenesis. The maximum error on the forecast charts also tended to be higher than those detected in the C.F.O. forecasts. Table II lists the means of these maximum errors for the 55 cases studied.

TABLE II. *Means of the maximum positive and negative errors in metres on each of 55 forecast charts.*

	Numerical forecasts		C.F.O. forecasts		Maximum 24-hour change	
	+ve	—ve	+ve	—ve	+ve	—ve
1000 mb	+139	—157	+104	—120	+132	—138
500–1000 mb	+150	—137	+120	—130	+147	—150
500 mb	+154	—137	+130	—160	+180	—192
200–500mb	+127	—108	+113	—108	+105	—116
200 mb	+180	—145	+146	—175	+186	—212

The magnitudes and locations of the maximum vector wind errors and changes were also noted and plotted for each forecast. The approximate positions of these maximum errors and changes (which relate to geostrophic winds measured over 1×1 grid length squares) are shown in Figures 3(*a*)–(*i*) for the 1000, 500 and 200 mb levels. At the 1000 mb level most of the maximum errors and changes occurred in the western half of the verification area; the similarity between the charts of C.F.O. errors and the maximum wind changes illustrates the tendency for forecasting errors to be at their greatest in regions of rapidly changing synoptic situations. The numerical forecasting errors (Figure 3(*a*)) show Greenland to be a region prone to large errors in the numerical prediction system. Some of the errors in this region are due to the effects of spurious anticyclogenesis towards the south-east and to the boundary assumptions, but the neglect of topography in the model is probably a principal contributor to this cluster of maximum errors over Greenland.

At the 500 mb level the effect of Greenland does not appear to be so significant, and at 200 mb the trend of maximum errors and changes to move southwards with height is clearly shown. The very large error of 177 knots in one of the numerical forecasts is partly due to instability in the computations, while the difficulty of constructing upper level charts with the existing radio-sonde network probably contributes to the cluster of errors and changes over the Mediterranean.

Thermal wind errors and changes are not included in the diagrams, but their salient features are somewhat similar to those of the contour charts. The numerically predicted 500–1000 mb thermal wind errors were particularly pronounced (up to 170 knots) over and just south of Greenland, while the 200–500 mb thermal wind errors were located mostly in the south and especially over the Mediterranean in the numerical forecasts.

THE "KINETIC ENERGY WIND ERROR"

A frequent fault in the numerical forecasts was the over-emphasis of contour gradients either due to the effects of spurious anticyclogenesis or due to the spurious introduction of

short-wave irregularities in the forecast patterns. A measure of the excessive forecast gradients was obtained by computing the square root of the mean of the differences between the squares of the forecast and actual geostrophic wind speeds measured over the 1×1 grid length squares of the verification area. The result of this computation may be expressed rather loosely but more descriptively as the amount by which forecast geostrophic wind speeds should be reduced in order to reduce the kinetic energy of the predicted flow to that of the actual geostrophic flow.

Table III shows the average of this "kinetic energy wind error", as it may be called, for the 55 cases studied in the experimental period.

TABLE III. *"Kinetic energy wind error" in knots*

	Numerical forecasts	C.F.O. forecasts
1000 mb	18	0
500–1000 mb	18	+1
500 mb	16	0
200–500 mb	14	−2
200 mb	20	+5

Obviously the numerical system builds up a considerable excess of kinetic energy at all levels in the forecasting process.

DISTRIBUTION OF MEAN ERRORS

Looking first at the 500 mb mean numerical error field (Figure 4(*e*)) we see that the numerical model has a marked tendency to predict excessively high contour heights over a large area extending from the Azores to Scandinavia while negative errors are centred at the southern tip of Greenland. Because the advection of the thickness patterns is very closely linked to the 500 mb flow, it is not surprising to find a tendency for warm air to be advected too far to the north in the numerical model—as shown—in Figures 4(*c*) and (*g*). Incorrect advection does not explain the mean positive 200–500 mb thickness errors in the neighbourhood of the Azores, but there is evidence (to be given on page 8) that these errors are associated with adiabatic warming by excessive descent of air in this region in the numerical model.

The 500 mb and the two thickness error fields combine to produce the distinctive M.S.L. and 200 mb error patterns shown in Figures 4(*a*) and (*i*). By comparison with the numerical error fields the C.F.O. errors are of much lower magnitudes and form less distinctive patterns at low levels. At high levels, however, there appears to be a significant tendency to predict excessively strong winds from the south-west across the Azores, while an error flow from the east near Greenland is probably due to underestimating the speed of the airstream from the west in this region.

DISTRIBUTION OF ROOT MEAN SQUARE ERRORS

The root mean square error fields computed for the 55 cases and displayed as Figures 5(*a*)–(*o*) show a distinct tendency for large C.F.O. forecasting errors to occur in regions where the 24-hour changes are large. The numerical root mean square error fields are also similar in pattern to the field of 24-hour changes in most regions excluding Greenland where the numerical forecasts are prone to large errors especially in the lower half of the troposphere.

CORRELATIONS BETWEEN FORECAST AND ACTUAL CHANGES

The distributions of mean correlation coefficients between the forecast and actual 24-hour changes are shown in Figures 6(*a*)–(*f*). In the neighbourhood of the British Isles both the numerical and the C.F.O. predicted changes were closely correlated with the actual 24-hour changes, but over Greenland and at high levels over the Mediterranean, both systems yielded low correlation coefficients for 24-hour changes. Marked differences between the two systems are shown at M.S.L. (Figures 6(*a*) and (*b*)) over Europe and over parts of the Atlantic. The numerical model appears to be relatively poor at predicting changes over Germany and France, probably because it neglects topography, friction and terrestrial temperature variations whose effects are built into the human forecaster's synoptic experience. In a broad band extending from the Azores to Iceland, however, the model appears to be superior to the conventional method of forecasting changes in the M.S.L. pattern; in other words, it is particularly efficient at handling the types of synoptic evolutions for which it is designed, that is, broad-scale development and movement over the sea.

ERRORS IN FORECASTING CENTRES OF LOW OR HIGH PRESSURE

In the 55 cases studied the numerical forecasts and the C.F.O. predictions included 53 and 74 low pressure centres respectively which could be identified with actual centres on the verification charts. High pressure centres totalling 26 on the numerical charts and 35 on the C.F.O. forecasts could also be easily identified with their corresponding centres on the actual charts. Tables IV and V show the distribution of displacement and intensity errors in forecasting these centres.

TABLE IV. *Distances of forecast low or high pressure centres from actual centres*

		Within 100 nautical miles	100–250 nautical miles	250–500 nautical miles	over 500 nautical miles
		percentages			
Low pressure centres	Numerical forecasts	32	36	32	0
	C.F.O. forecasts	33	33	34	0
High pressure centres	Numerical forecasts	35	35	22	8
	C.F.O. forecasts	31	34	29	6

TABLE V. *Errors in forecasting depths of depressions and intensity of anticyclones*

		too low				too high				Mean pressure error
		over 15 mb	10–15 mb	5–10 mb	0–5 mb	0–5 mb	5–10 mb	10–15 mb	over 15 mb	
		percentages								
Low pressure centres	Numerical forecasts	21	23	23	25	6	1	1	0	8 mb too low
	C.F.O. forecasts	12	16	25	34	11	2	0	0	6 mb too low
High pressure centres	Numerical forecasts	0	0	12	27	30	27	0	4	3 mb too high
	C.F.O. forecasts	0	0	8	54	35	3	0	0	1 mb too low

The displacement errors in forecasting low or high pressure centres revealed no significantly preferred direction; the C.F.O. displacement errors were grouped fairly uniformly around the actual centres and the numerical method showed a slight, but scarcely significant, tendency to move depression centres too far towards the north. Table V shows the marked tendency for numerically predicted depressions to be too deep while anticyclones are often too intense. Although the number of anticyclones in the sample was small (only 26) the distribution of error frequencies illustrates a feature of spurious anticylogenesis that was noticed during subjective assessment of the forecasts, namely that spurious anticyclogenesis appears to be an unstable process; spurious intensification appears to take place to either a moderate degree or to a synoptically unrealistic extent with few cases between these descriptive ranges.

CONTINUITY OF ERROR PATTERNS

Although the numerical model showed no systematic displacement errors in predicting the movement of depressions and high pressure centres when the whole four-month experimental period is considered, it is pertinent to inquire whether any continuity of error pattern was detectable over shorter periods of, say, a few days. Figures 7(*a*), (*b*) and (*c*) illustrate both continuity and erratic behaviour of the day-to-day error pattern. In this three-day sequence we see that, broadly speaking, the depressions which moved eastwards across the northern half of the verification area were accompanied by negative errors with maxima west or north-west of the predicted centres. Thus in this region there was some recognizable error pattern linked with the low pressure systems in this particular three-day sequence. The positive error pattern associated with the high pressure system towards the south, however, was quite erratic in its day-to-day behaviour. These three charts are typical of the error sequences studied; in fact they virtually summarize the subjectively acquired view that although some day-to-day continuity of error pattern is usually discernible, it is often vague and unreliable as a guide to correcting a forecast empirically.

VERTICAL MOTION FIELDS

The products of the computing procedure included fields of mean vertical motion for the two layers 1000–600 mb and 200–600 mb. Figures 8(*a*) and (*b*) show the mean of all the fields corresponding to the 55 24-hour forecasts, while charts (*c*) and (*d*) of the figure show the "verifying" charts, or more precisely the mean of the vertical motion fields computed for the verifying contour and thickness charts.

The very broad features of the forecast and "actual" computed mean vertical motion are similar; ascent of air near Newfoundland and in a broad belt from Greenland to the Bay of Biscay and descent west of Greenland, near the Azores and over the Baltic are noticeable on all four charts. The principal errors in the mean forecast charts appear to be the spurious tongue of descent north of the Azores and underestimation of the extent of a cell of mean descent centred over Spain and extending to south-west France. Probably these errors are associated with spurious anticyclogenesis and topography respectively. In addition to these particular features the numerical model exaggerates the mean vertical motion.

CONCLUSIONS

The principal features which emerge from this study of error fields may be summarized as follows:

(*i*) On average the geographical distribution of errors in the numerical and conventional forecasts have much in common.

(*ii*) The principal type of numerical forecasting error appears to be spurious anticyclogenesis at the middle level of the model with spurious cyclogenesis at M.S.L. being a very significant associated effect.

(*iii*) Although synoptically significant boundary effects have impaired predictions within the verification area on a few occasions, these effects do not appear to pose a major problem within this area for 24-hour forecasts.

(*iv*) Neglect of topography appears to produce large errors and low correlation coefficients for 24-hour forecast and actual changes in the neighbourhood of Greenland, while over central Europe the omission of topographical effects is reflected mainly by very poor correlations.

(*v*) Broadly speaking the numerical forecasts tend to over-emphasize the west–east flow especially in the west. Spurious small-scale undulations in the predicted flow patterns together with the excessive flow from the west lead to a marked increase of kinetic energy in nearly all of the forecast patterns.

(*vi*) The regions prone to maximum geostrophic wind errors shift southwards with height. At M.S.L. large wind errors are concentrated over Greenland; at the 200 mb level wind errors are particularly pronounced near the Azores and over the Mediterranean. The numerical and C.F.O. maximum wind error patterns are very similar, but at high levels spurious undulations in the numerically predicted flow occasionally produced very large errors in winds measured over one grid length.

(*vii*) A day-to-day continuity of error pattern is usually discernible but it is often vague and unreliable as a guide to correcting a forecast empirically.

(*viii*) The numerical model exaggerates the computed vertical motion averaged over a number of forecasts.

(*ix*) The model appears to be efficient at predicting broad-scale development and movement of pressure contour features over the sea some distance away from land masses and from the boundary of the computing area.

BIBLIOGRAPHY

1. BUSHBY, F. H. and WHITELAM, C. J.; A three-parameter model of the atmosphere suitable for numerical integration. *Quart. J. R. met. Soc., London*, **87**, 1961, p. 374.

2. CRADDOCK, J. M.; The warming of arctic air masses over the eastern North Atlantic. *Quart. J. R. met. Soc., London*, **77**, 1951, p. 355.

3. KNIGHTING, E., CORBY, G. A., BUSHBY, F. H. and WALLINGTON, C. E.; An experiment in numerical forecasting. *Sci. Pap., met. Off., London*, No. 5, 1961.

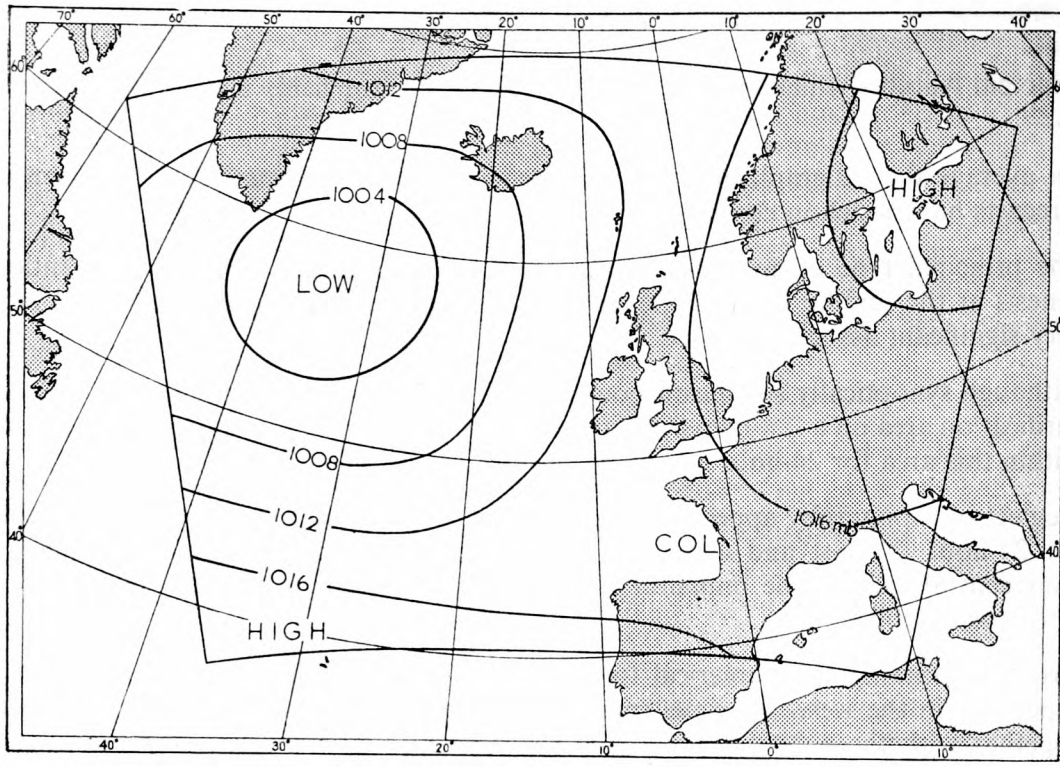

FIGURE 2(*a*). Average M.S.L. pressure pattern in millibars for 55 24-hour forecast periods studied

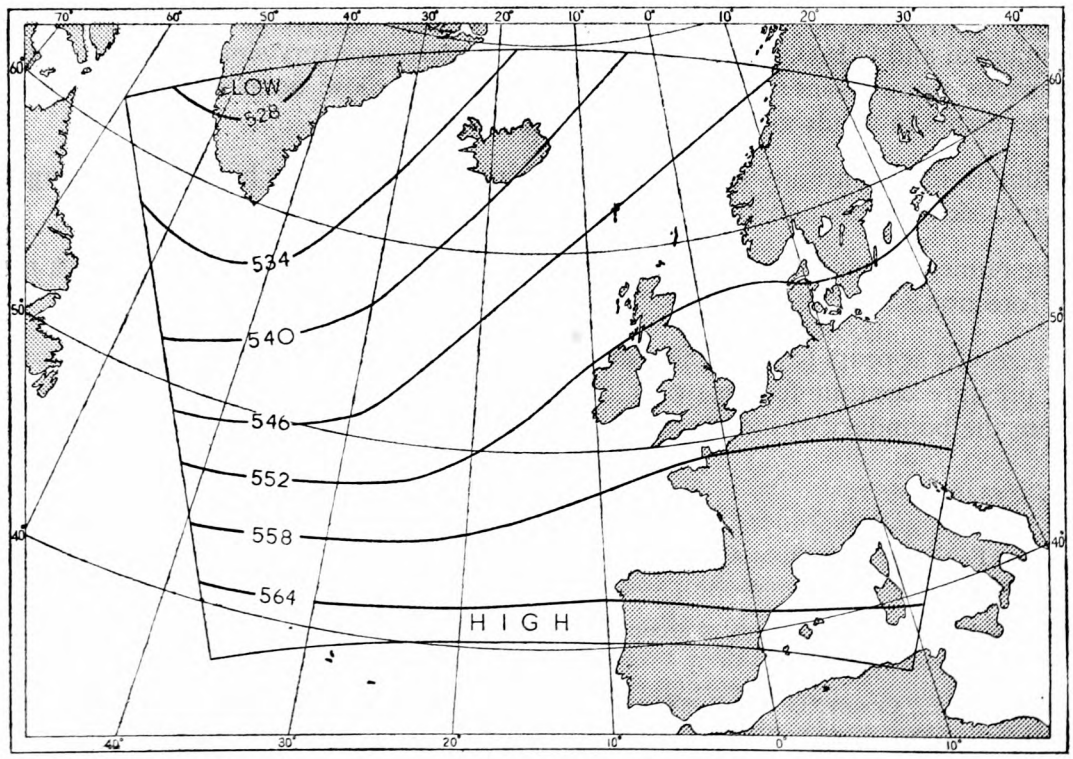

FIGURE 2(*b*). Average 500 mb contour pattern in tens of metres for 55 24-hour forecast periods studied

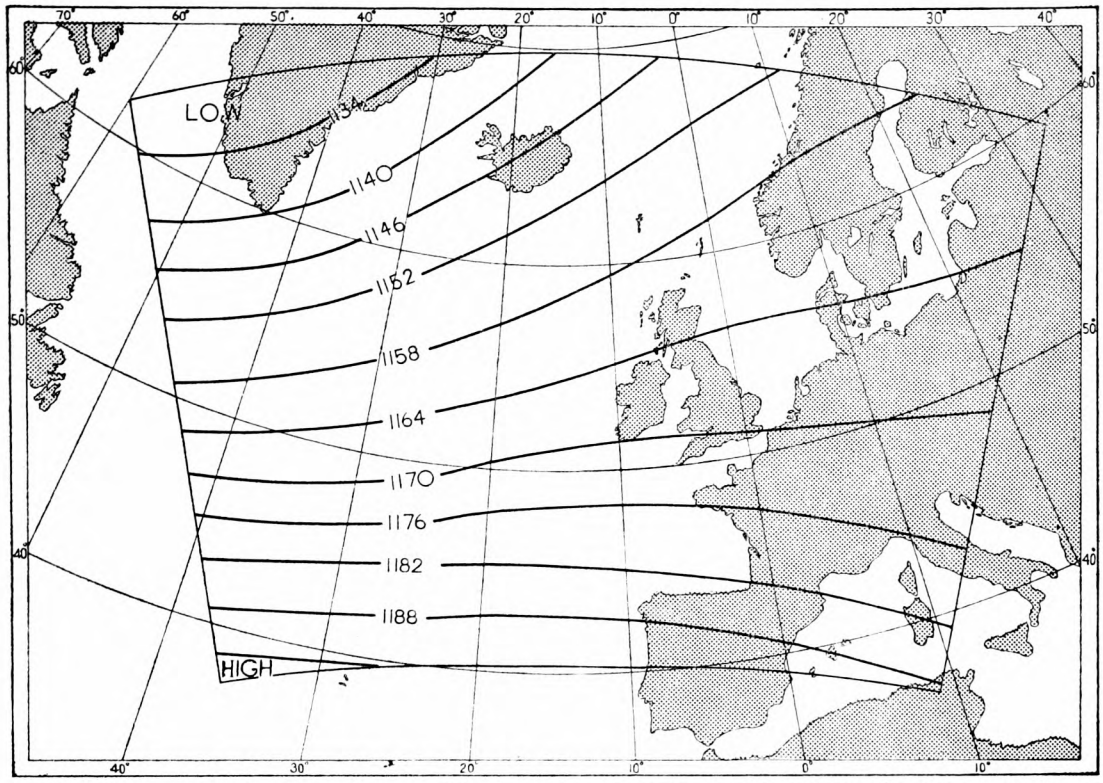

FIGURE 2(*c*). Average 200 mb contour pattern in tens of metres for 55 24-hour forecast periods studied

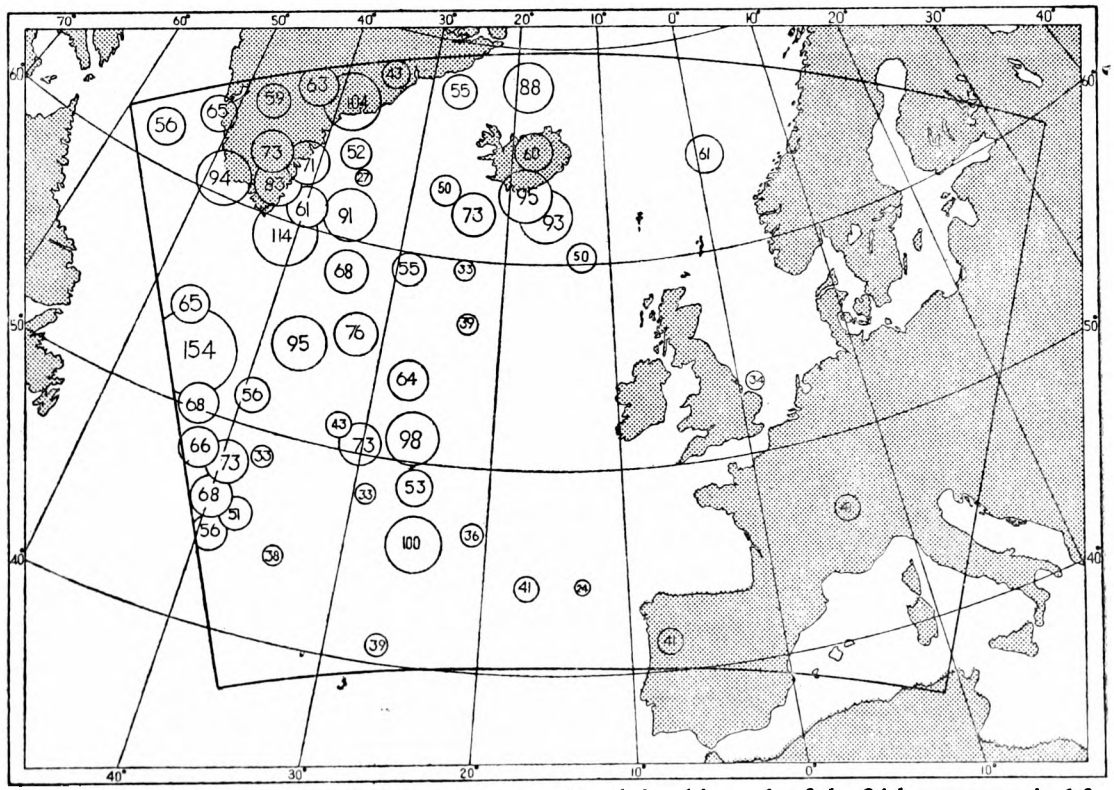

FIGURE 3(*a*). Maximum geostrophic wind errors at 1000 mb level in each of the 24-hour numerical forecasts Positions of circles show the approximate locations; vector magnitudes of errors are denoted by inscribed numbers (in knots) and are proportional to diameters of the circles. There were 55 cases in the period 29 Feb.–2 June 1960.

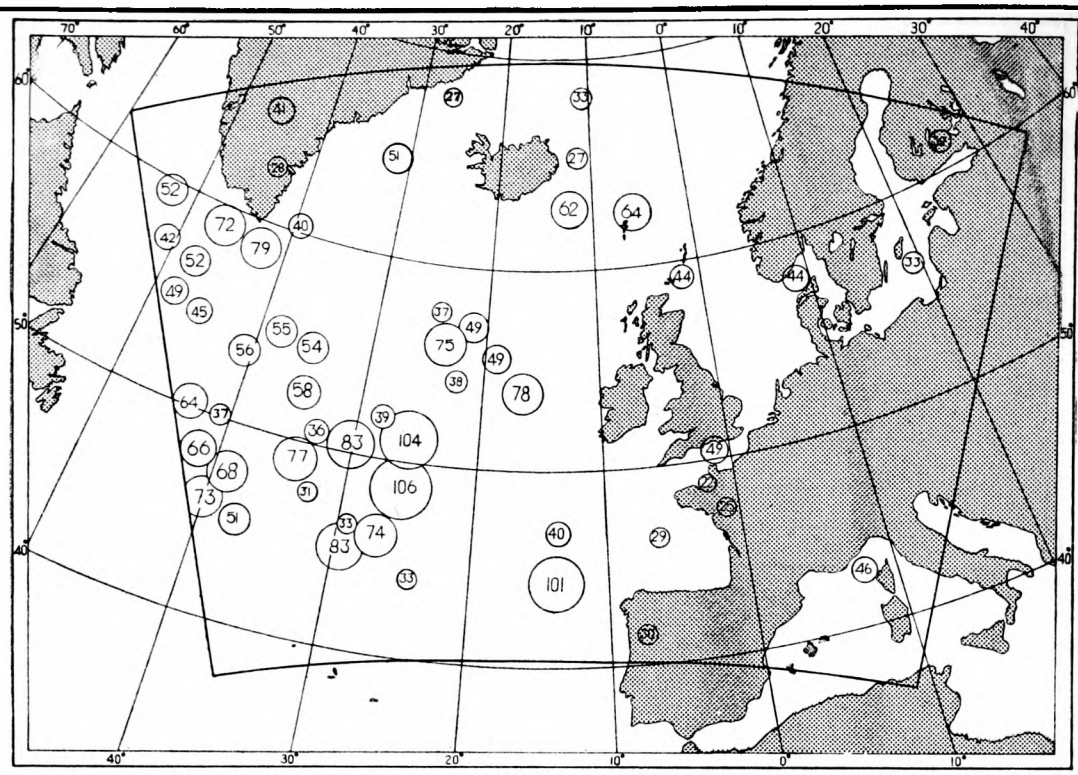

FIGURE 3(*b*). Maximum geostrophic wind errors at 1000 mb level in each of the 24-hour C.F.O. forecasts Positions of circles show the approximate locations; vector magnitudes of errors are denoted by inscribed numbers (in knots) and are proportional to diameters of the circles.

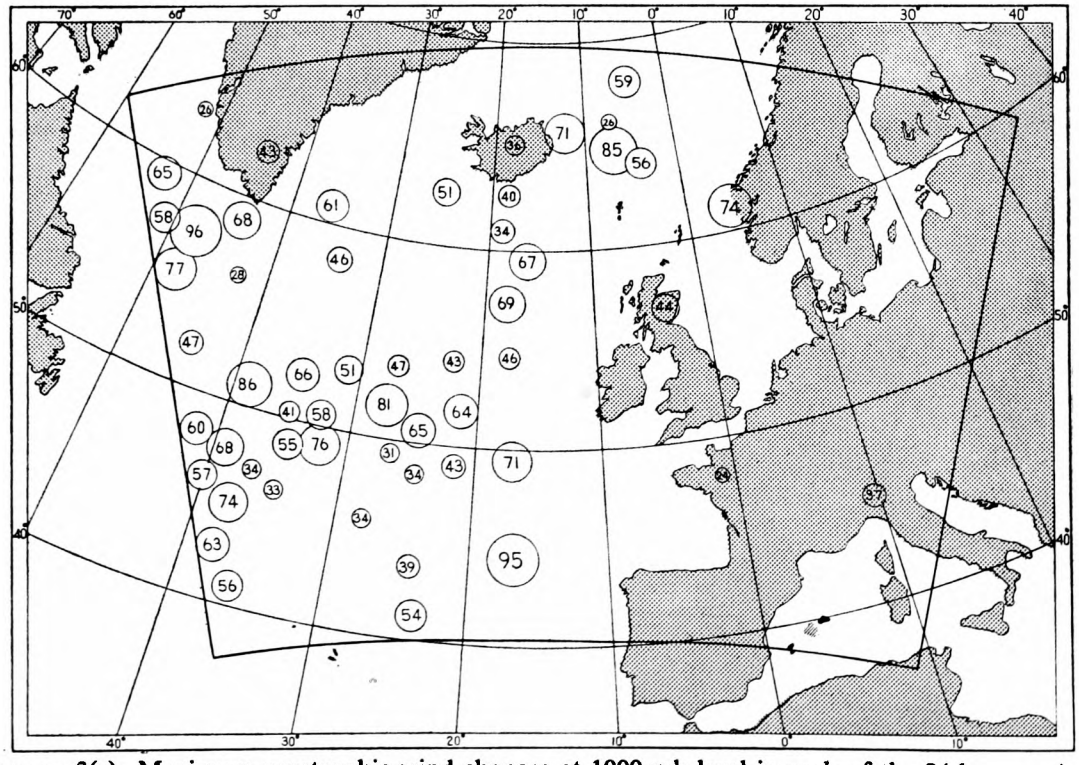

FIGURE 3(*c*). Maximum geostrophic wind changes at 1000 mb level in each of the 24-hour periods Positions of circles show the approximate locations; vector magnitudes of changes are denoted by inscribed numbers (in knots) and are proportional to diameters of the circles.

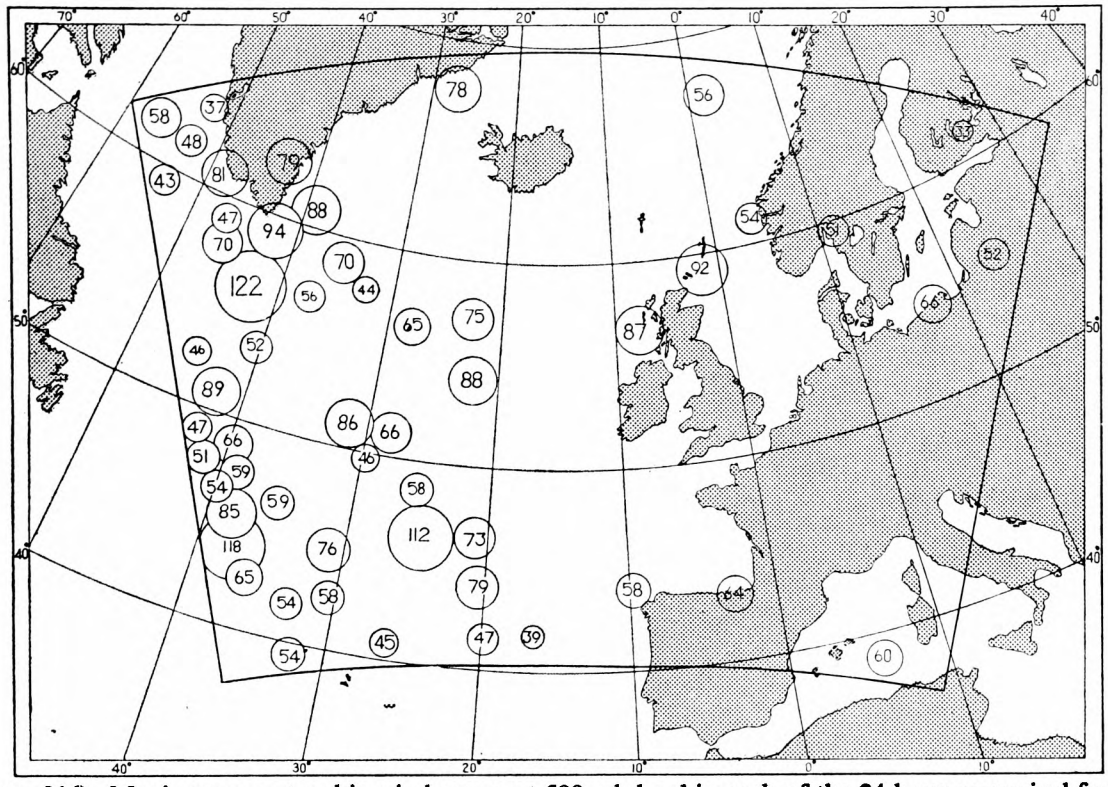

FIGURE 3(*d*). Maximum geostrophic wind errors at 500 mb level in each of the 24-hour numerical forecasts Positions of circles show the approximate locations; vector magnitudes of errors are denoted by inscribed numbers (in knots) and are proportional to diameters of the circles.

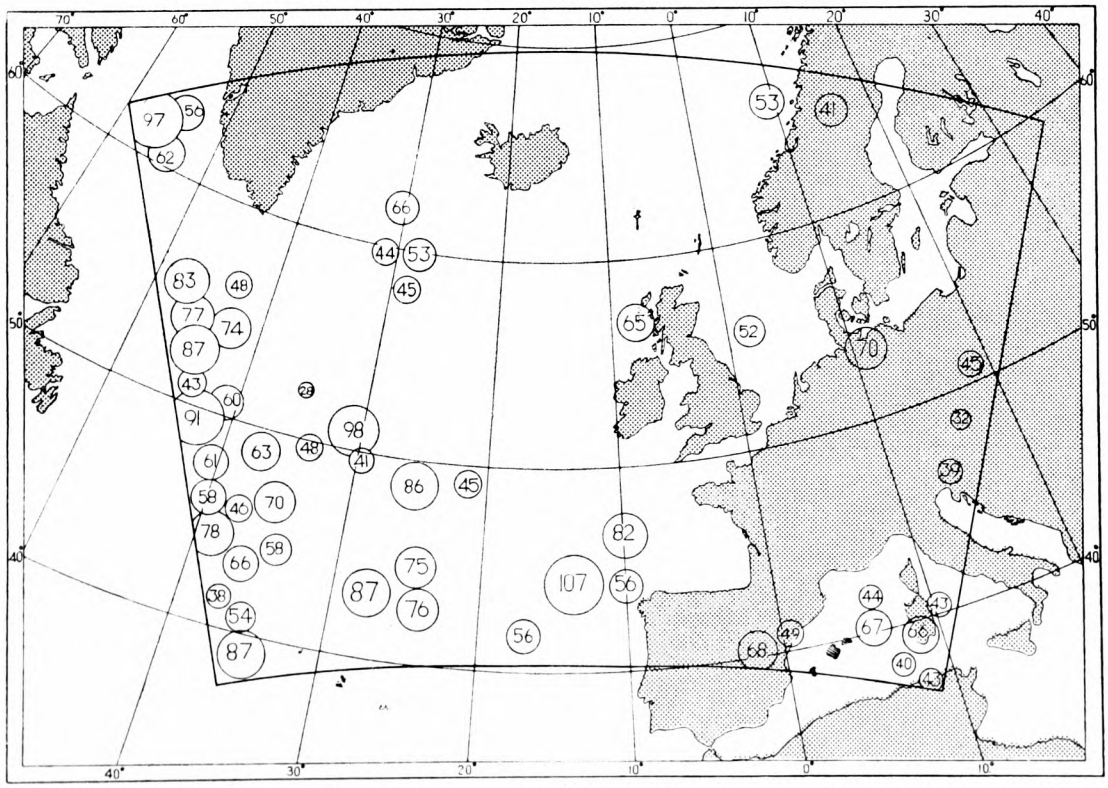

FIGURE 3(*e*). Maximum geostrophic wind errors at 500 mb level in each of the 24-hour C.F.O. forecasts Positions of circles show the approximate locations; vector magnitudes of errors are denoted by inscribed numbers (in knots) and are proportional to diameters of the circles.

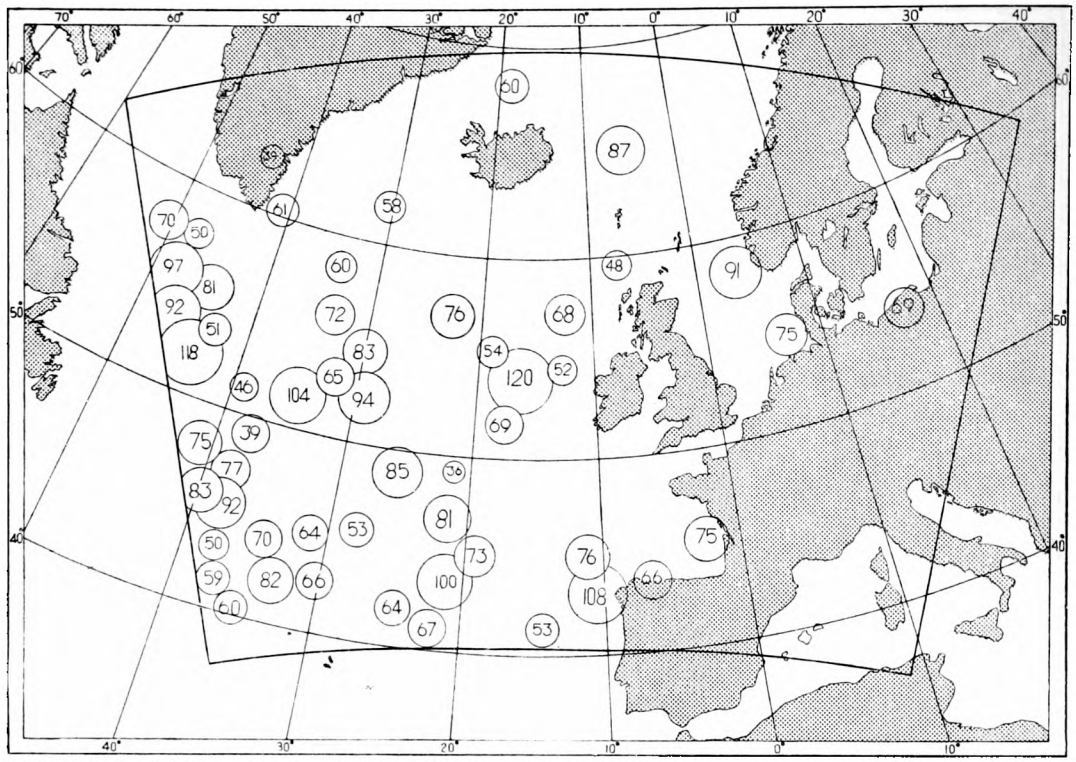

FIGURE 3(*f*). Maximum geostrophic wind changes at 500 mb level in each of the 24-hour periods Positions of circles show the approximate locations; vector magnitudes of changes are denoted by inscribed numbers (in knots) and are proportional to diameters of the circles.

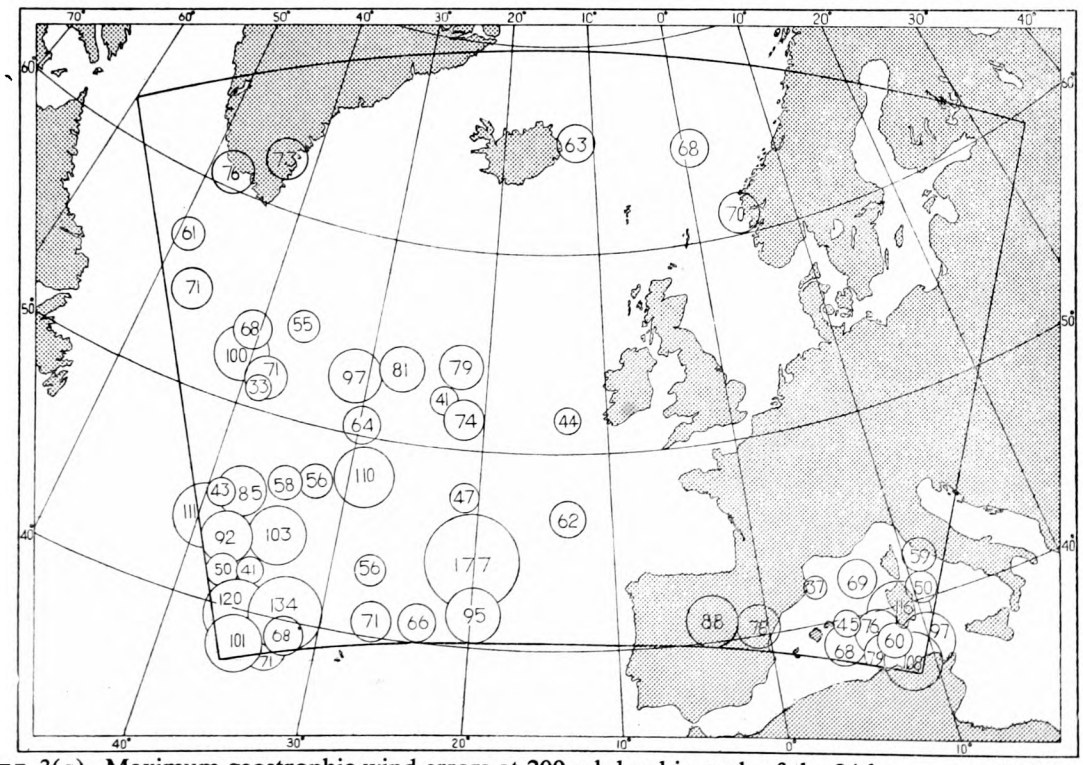

FIGURE 3(*g*). Maximum geostrophic wind errors at 200 mb level in each of the 24-hour numerical forecasts Positions of circles show the approximate locations; vector magnitudes of errors are denoted by inscribed numbers (in knots) and are proportional to diameters of the circles.

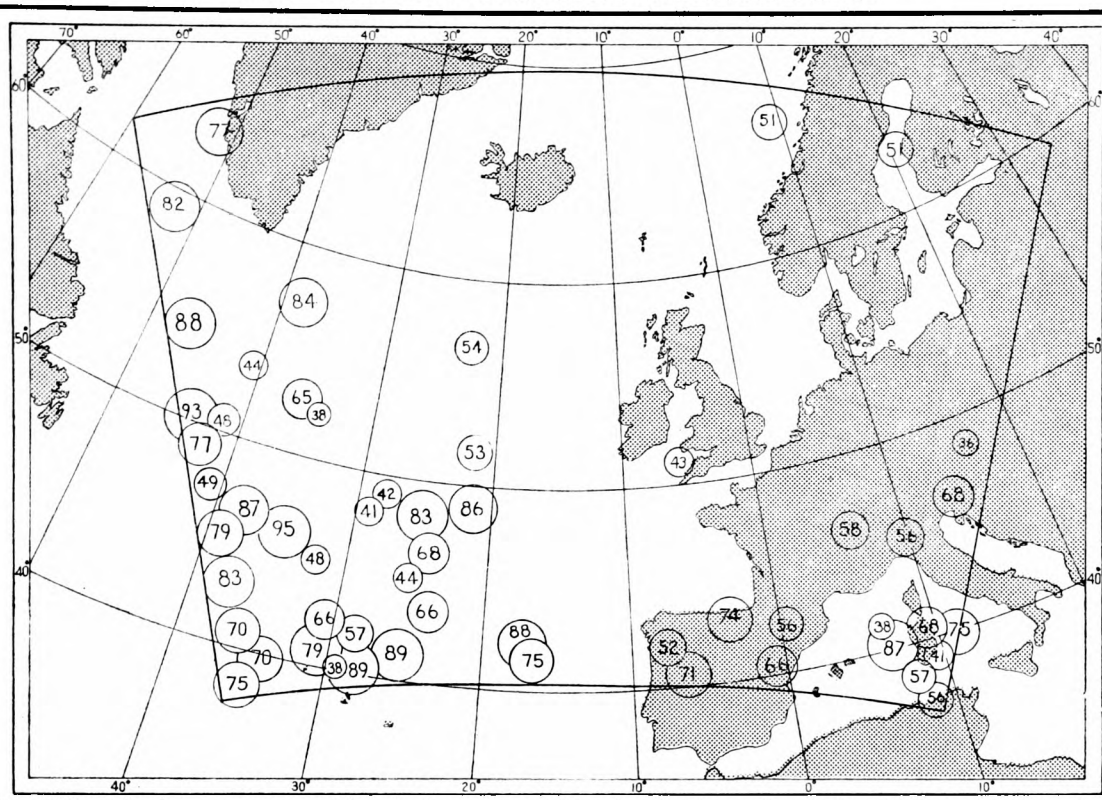

FIGURE 3(*h*). Maximum geostrophic wind errors at 200 mb level in each of the 24-hour C.F.O. forecasts Positions of circles show the approximate locations; vector magnitudes of errors are denoted by inscribed numbers (in knots) and are proportional to diameters of the circles.

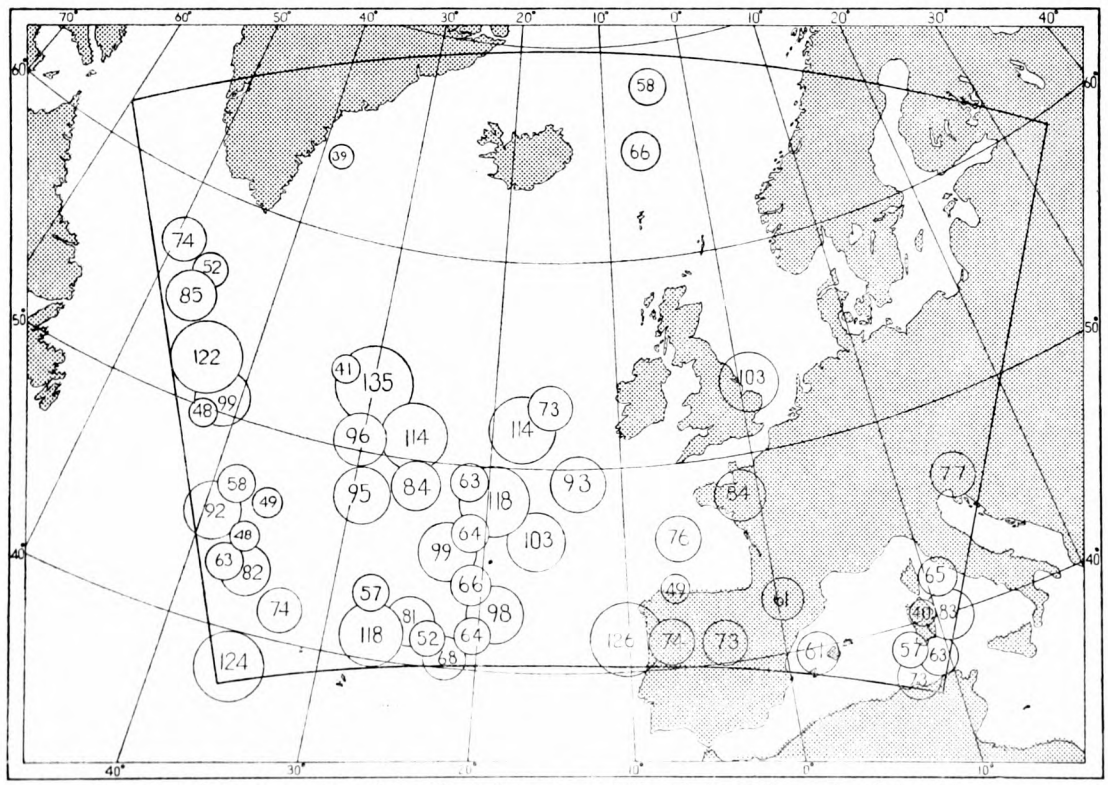

FIGURE 3(*i*). Maximum geostrophic wind changes at 200 mb level in each of the 24-hour periods Positions of circles show the approximate locations; vector magnitudes of changes are denoted by inscribed numbers (in knots) and are proportional to diameters of the circles.

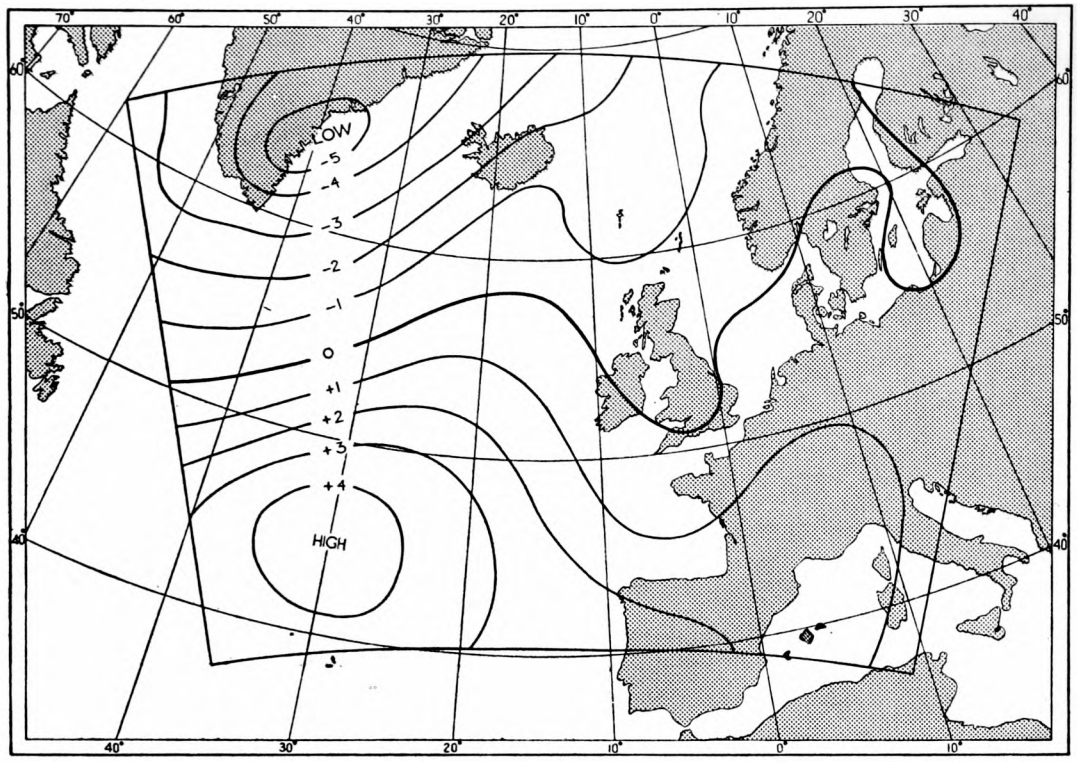

FIGURE 4(*a*). Average M.S.L. pressure errors (numerical forecast—actual values in millibars) in the 55 24-hour forecasts studied. Period 29 Feb.–2 June 1960.

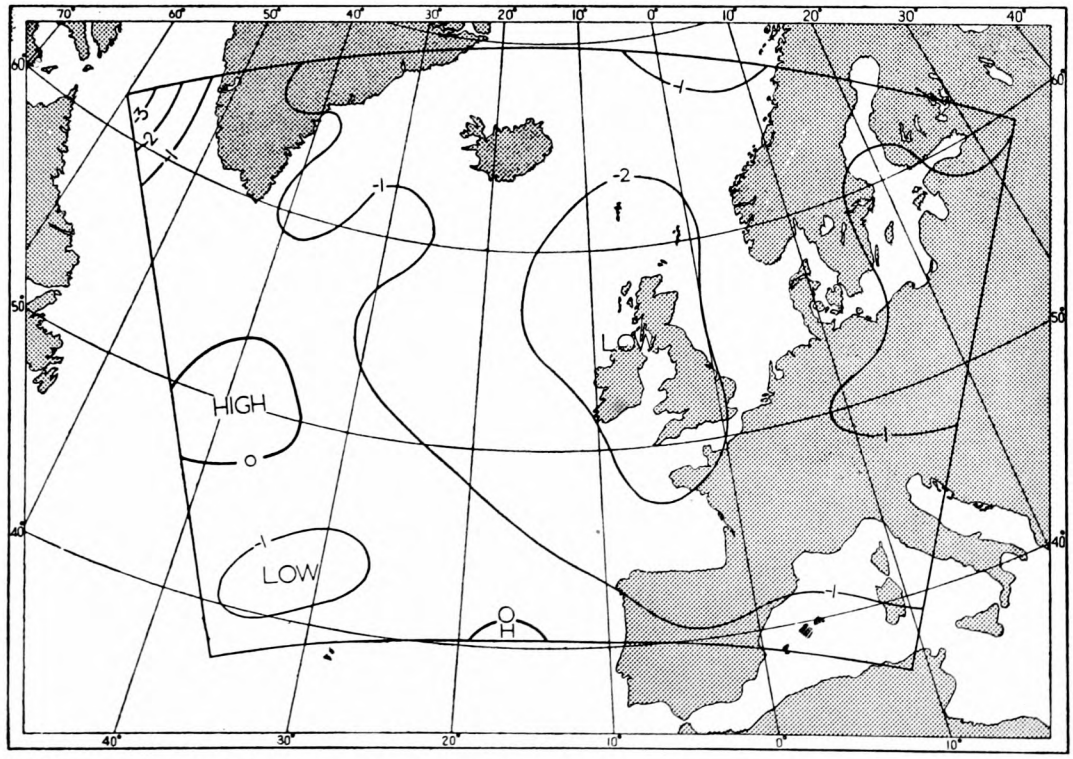

FIGURE 4(*b*). Average M.S.L. pressure errors (C.F.O. forecast—actual values in millibars) in the 55 24-hour forecasts studied

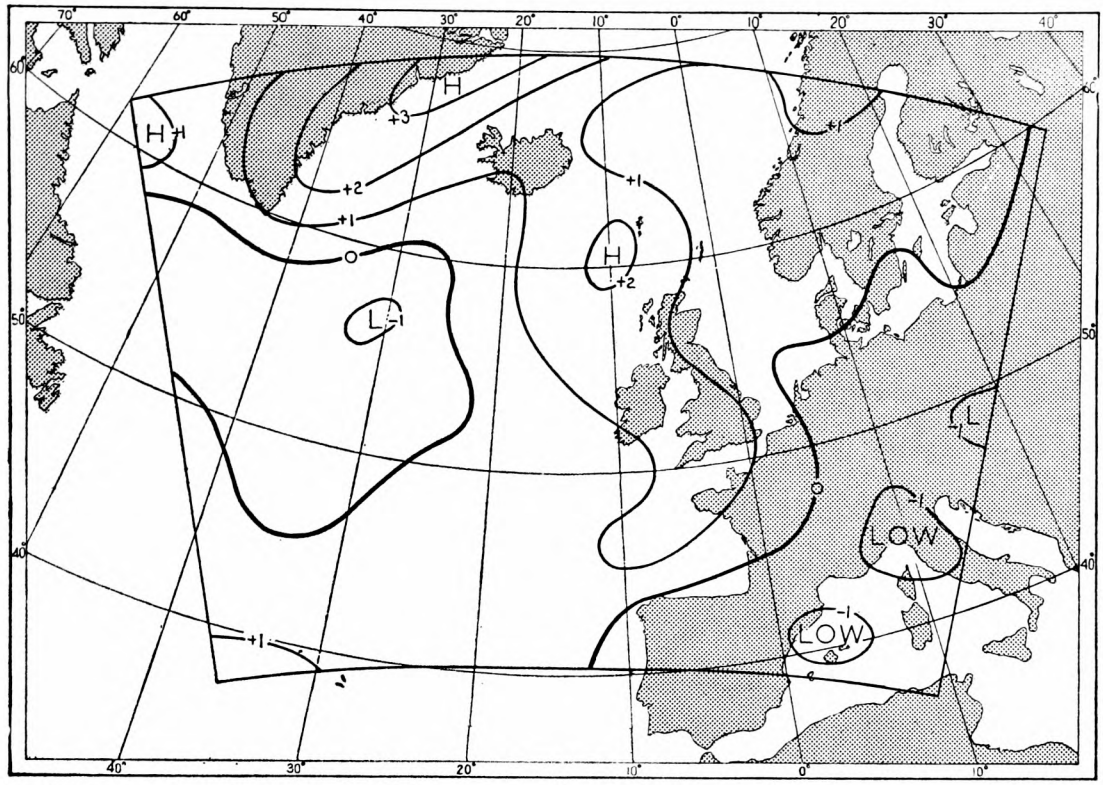

FIGURE 4(*c*). Average 500–1000 mb thickness errors (numerical forecasts—actual values in tens of metres) in the 55 24-hour forecasts studied

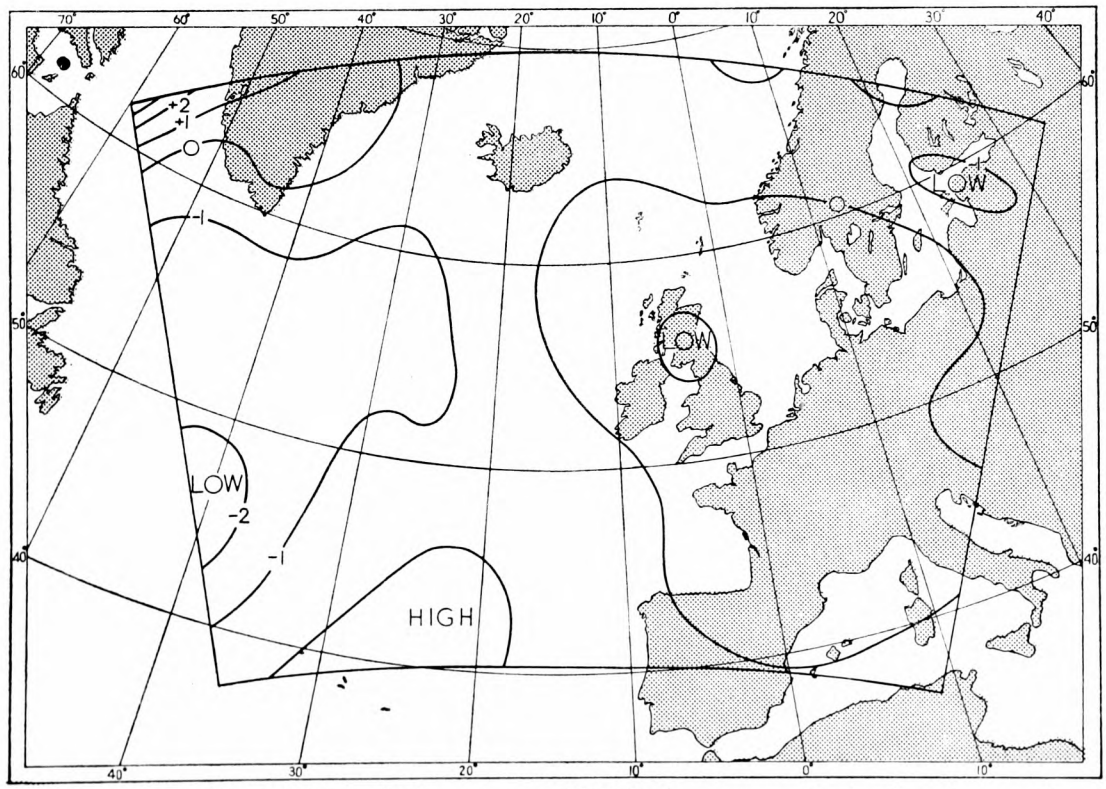

FIGURE 4(*d*). Average 500–1000 mb thickness errors (C.F.O. forecasts—actual values in tens of metres) in the 55 24-hour forecasts studied

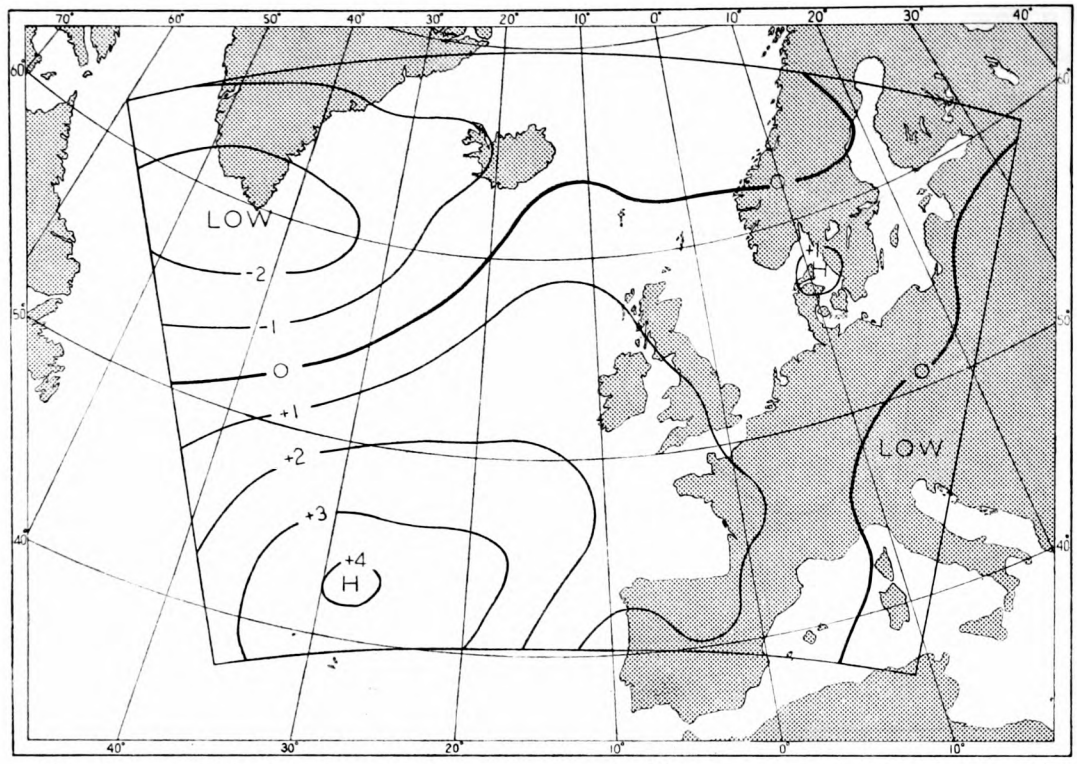

FIGURE 4(*e*). Average 500 mb contour height errors (numerical forecasts—actual values in tens of metres) in the 55 24-hour forecasts studied

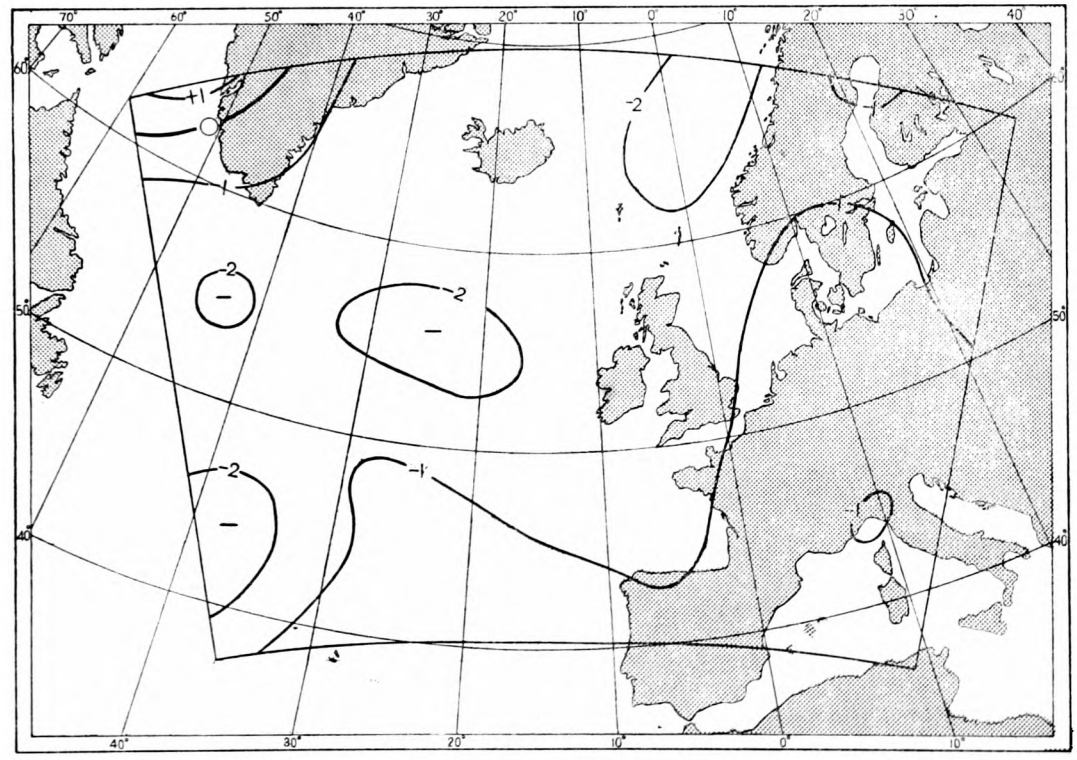

FIGURE 4(*f*). Average 500 mb contour height errors (C.F.O. forecasts—actual values in tens of metres) in the 55 24-hour forecasts studied

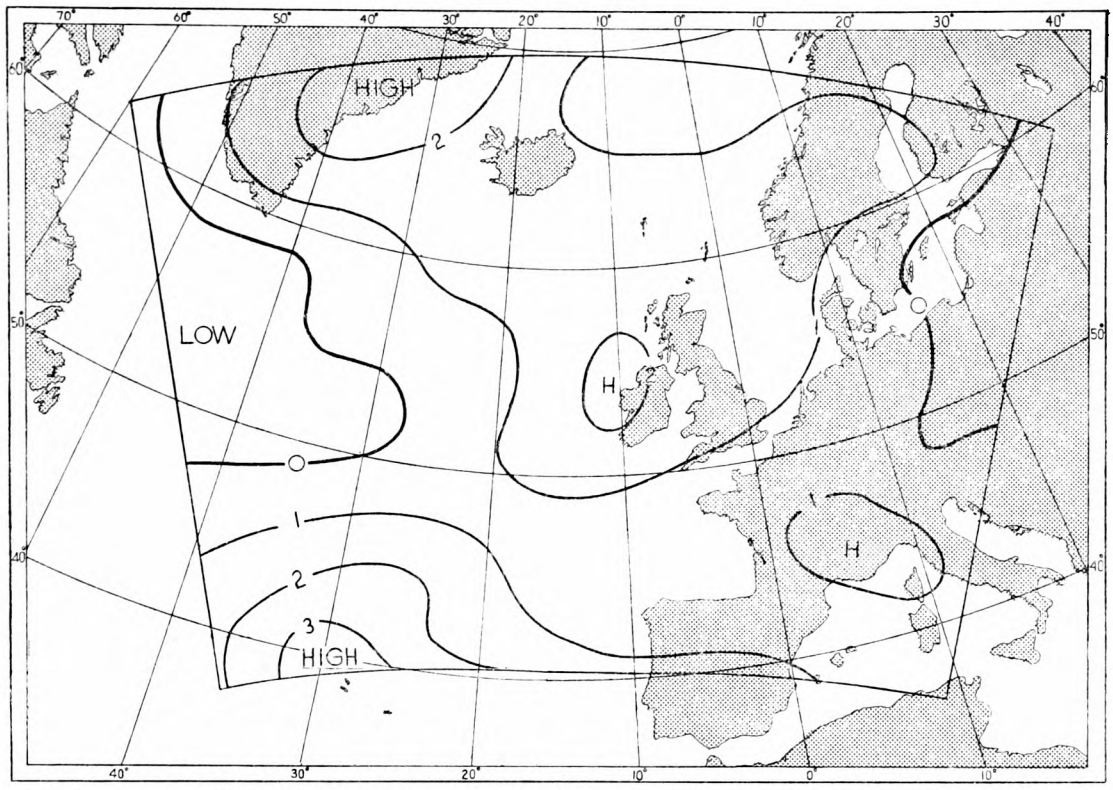

FIGURE 4(*g*). Average 200–500 mb thickness errors (numerical forecasts—actual values in tens of metres) in the 55 24-hour forecasts studied

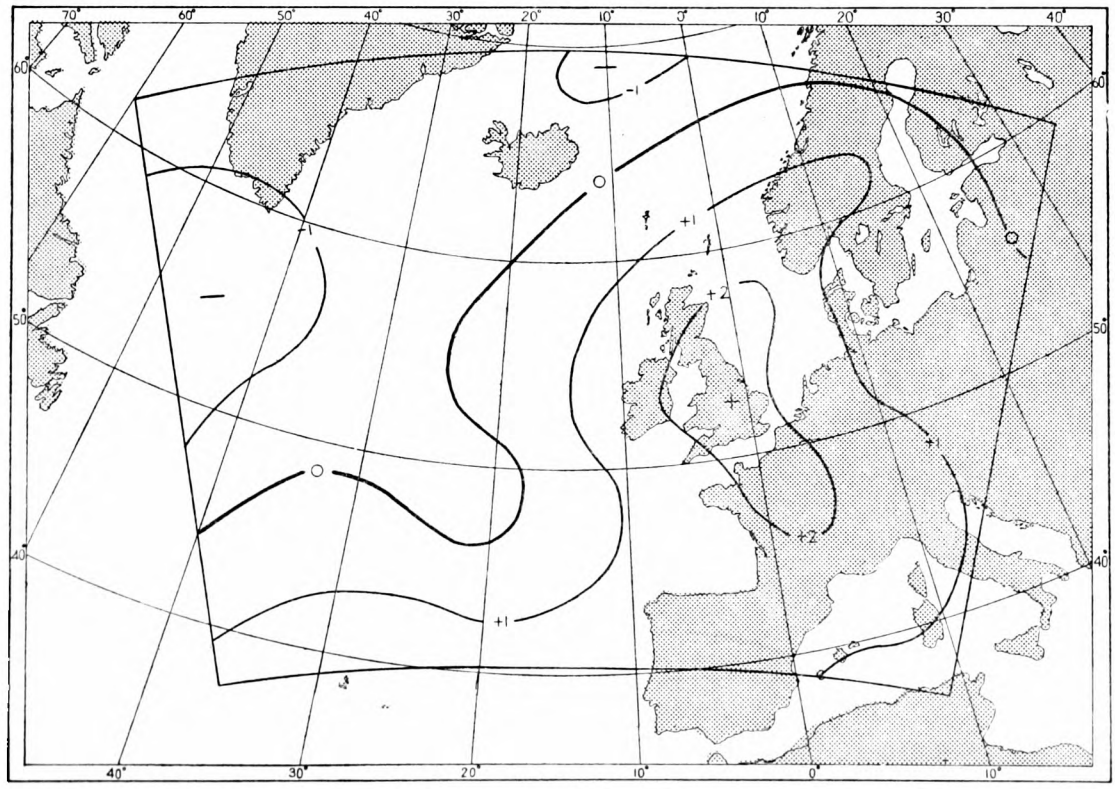

FIGURE 4(*h*). Average 200–500 mb thickness errors (C.F.O. forecasts—actual values in tens of metres) in the 55 24-hour forecasts studied

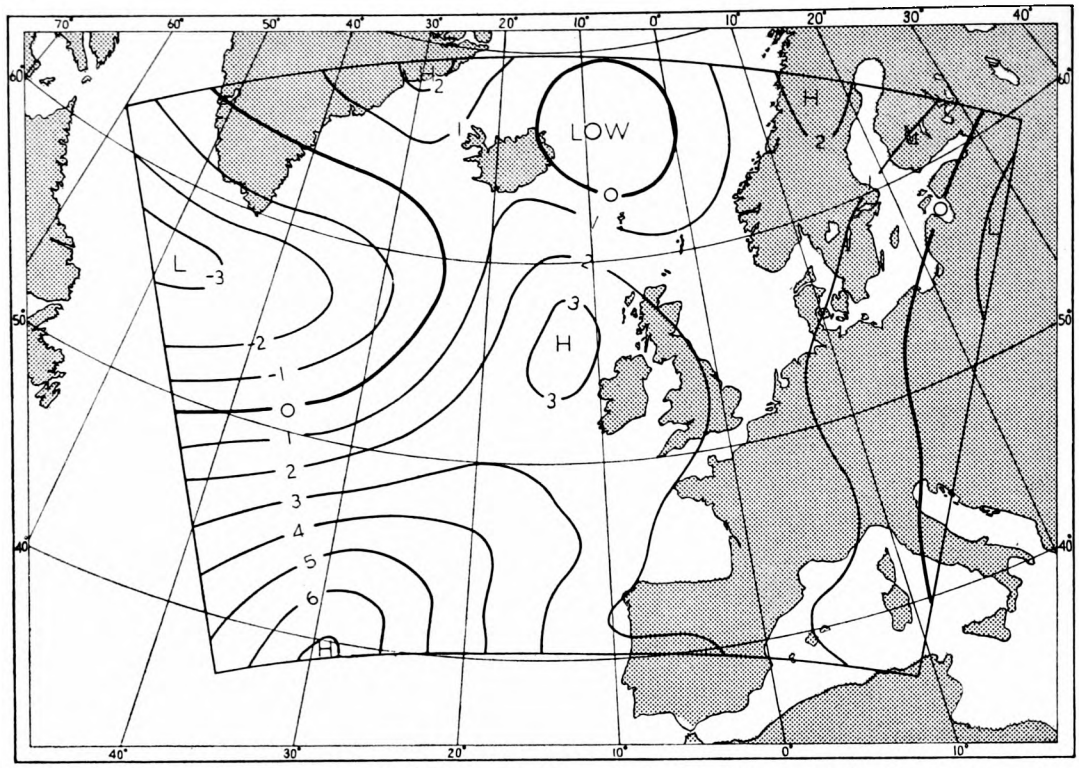

FIGURE 4(*i*). Average 200 mb contour height errors (numerical forecasts—actual values in tens of metres) in the 55 24-hour forecasts studied

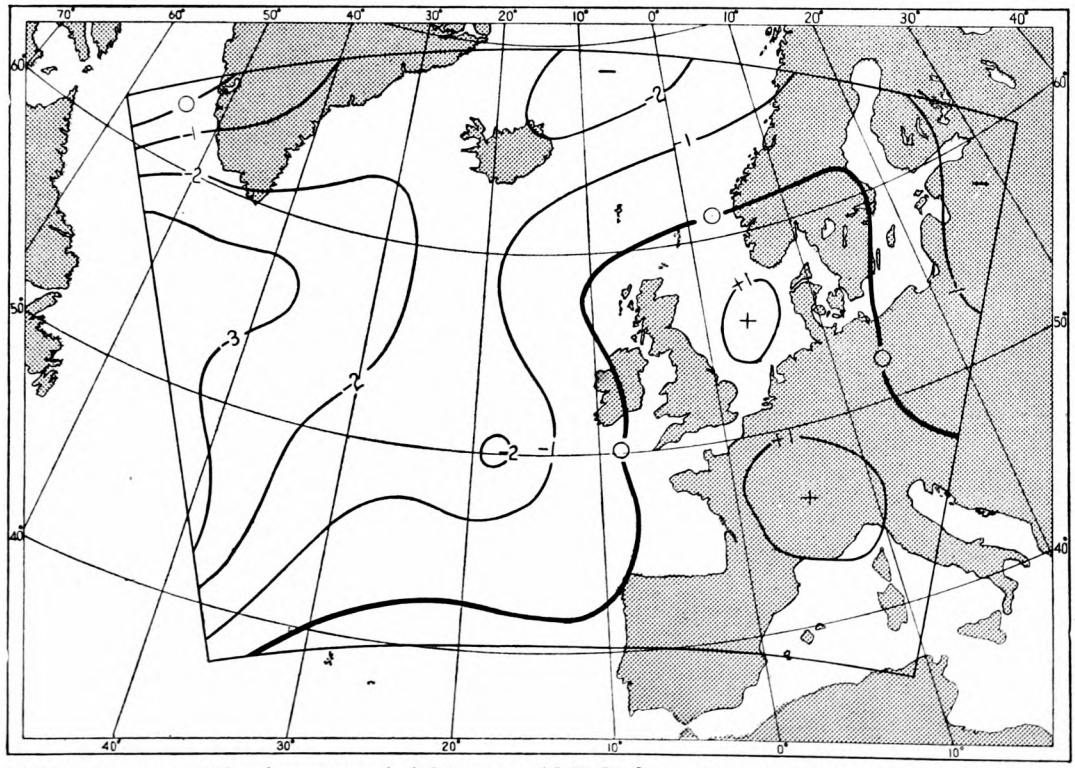

FIGURE 4(*j*). Average 200 mb contour height errors (C.F.O. forecasts—actual values in tens of metres) in the 55 24-hour forecasts studied

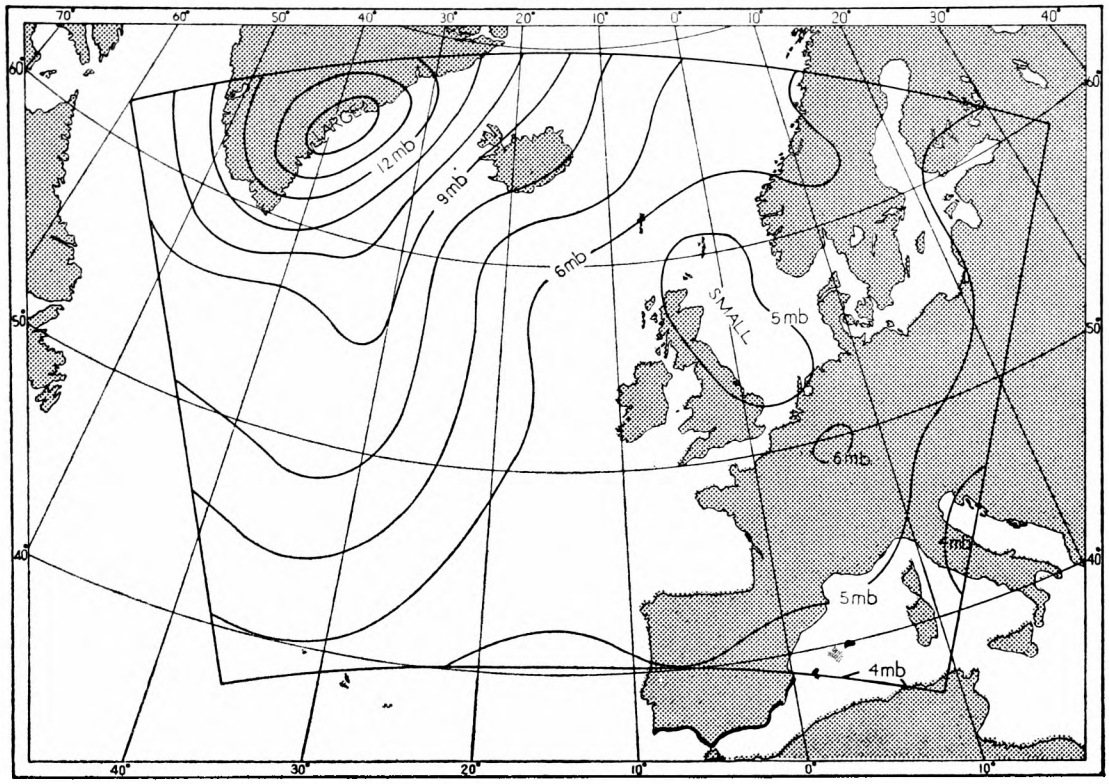

FIGURE 5(*a*). Root mean square M.S.L. pressure errors in millibars, 24-hour numerical forecasts, 55 cases in the period 29 Feb.–2 June 1960

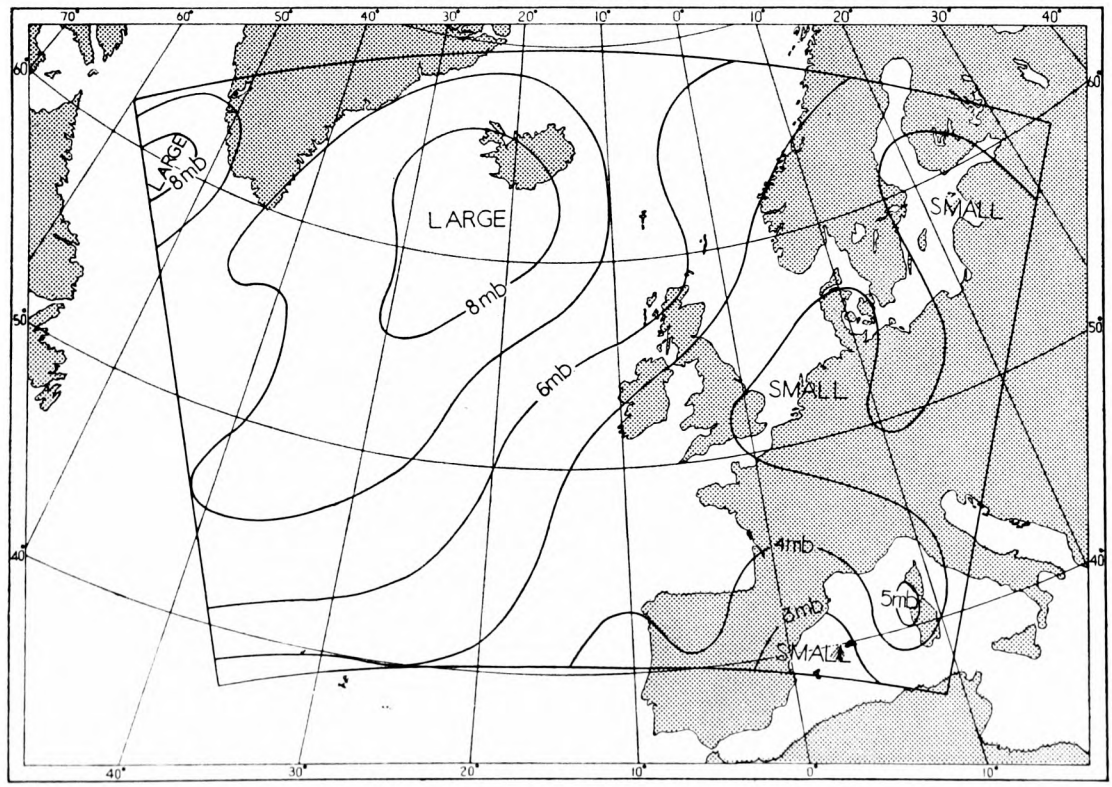

FIGURE 5(*b*). Root mean square M.S.L. pressure errors in millibars, 24-hour C.F.O. forecasts

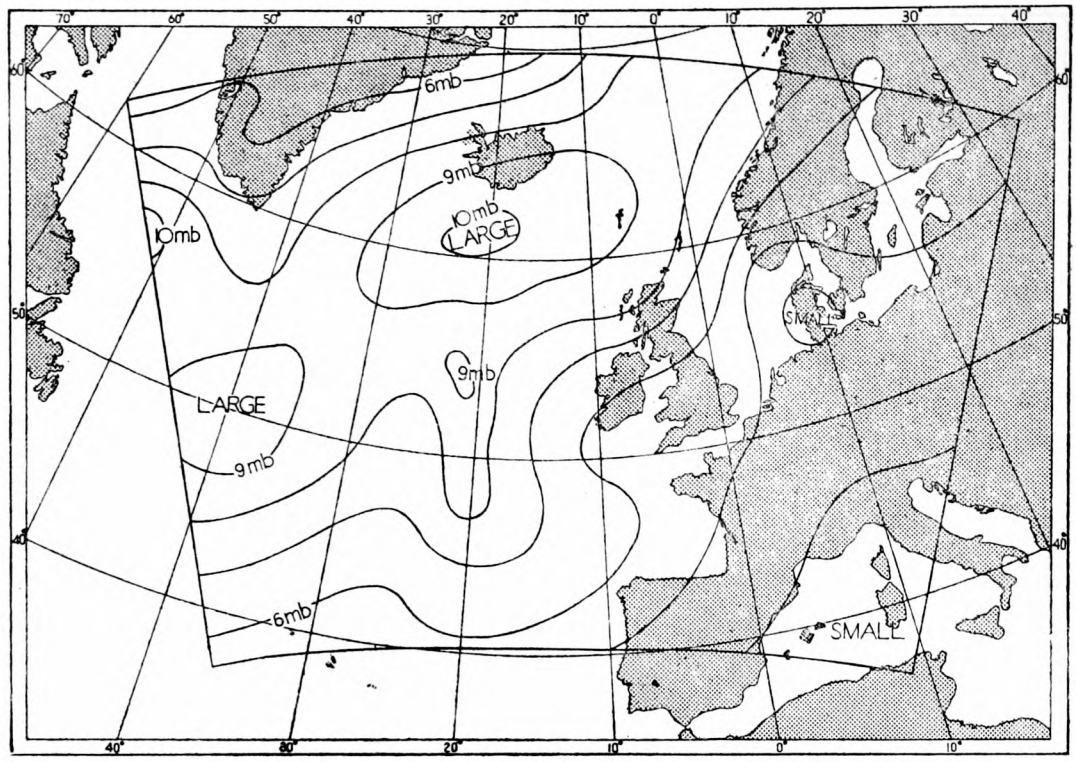

FIGURE 5(*c*). Root mean square M.S.L. pressure changes in millibars, 24-hour periods

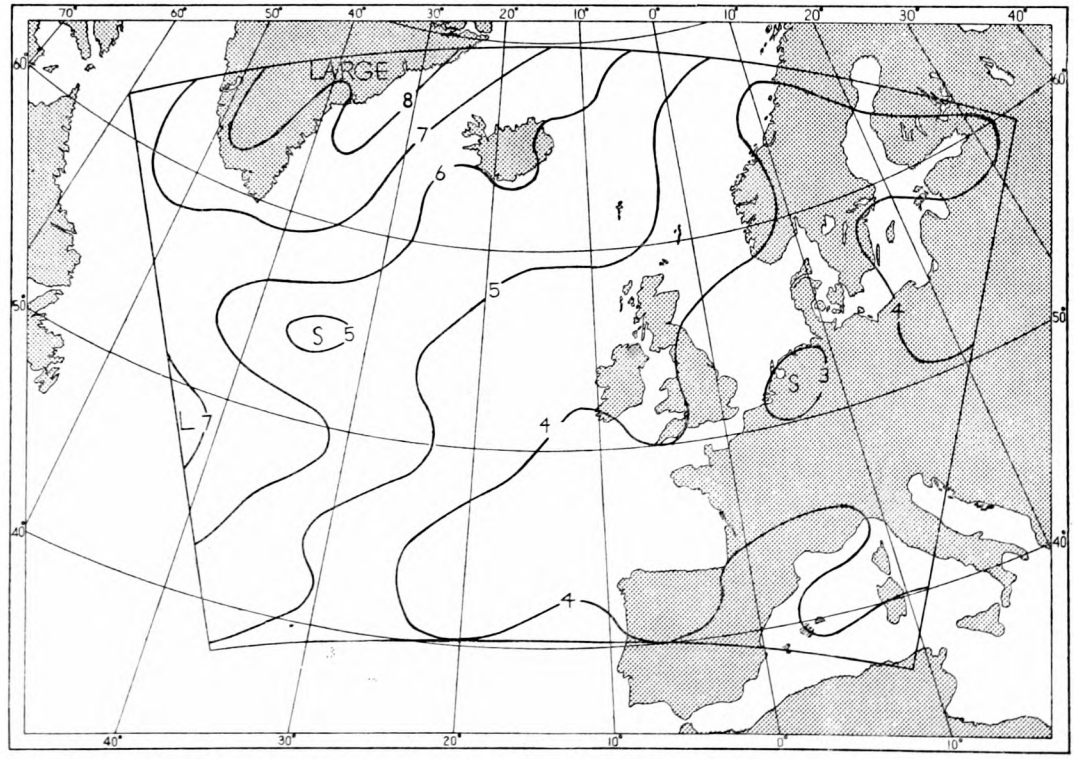

FIGURE 5(*d*). Root mean square 500–1000 mb thickness errors in tens of metres, 24-hour numerical forecasts

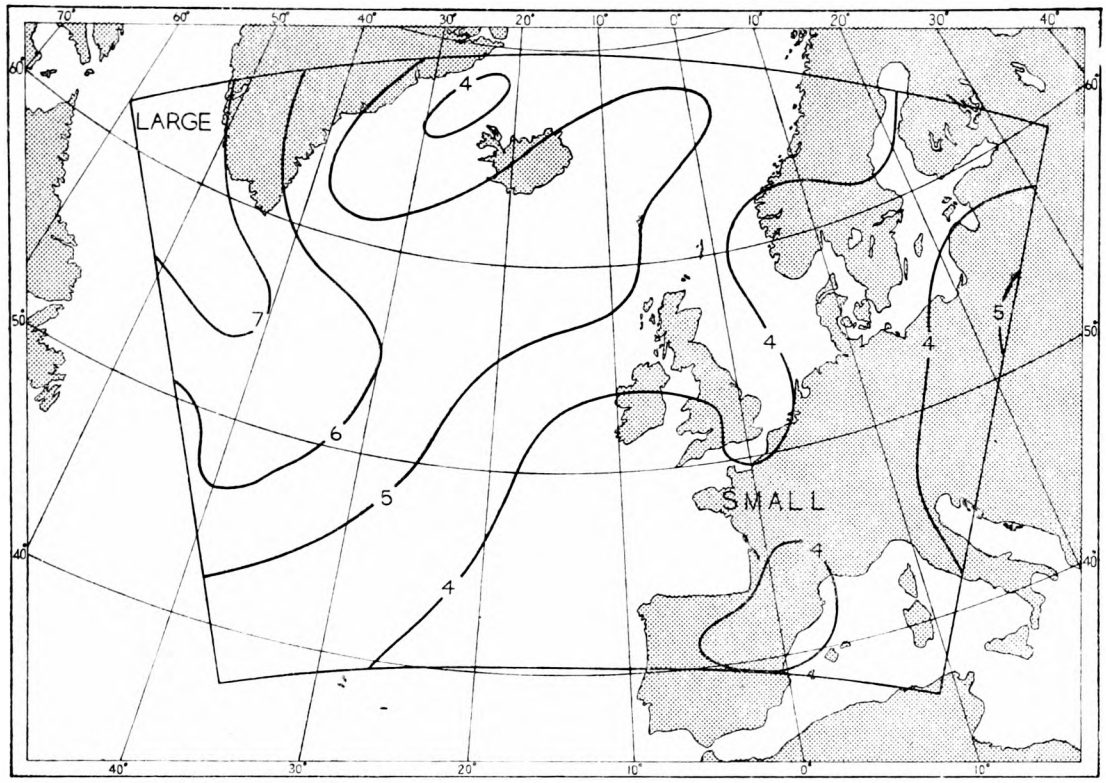

FIGURE 5(*e*). Root mean square 500–1000 mb thickness errors in tens of metres, 24-hour C.F.O. forecasts

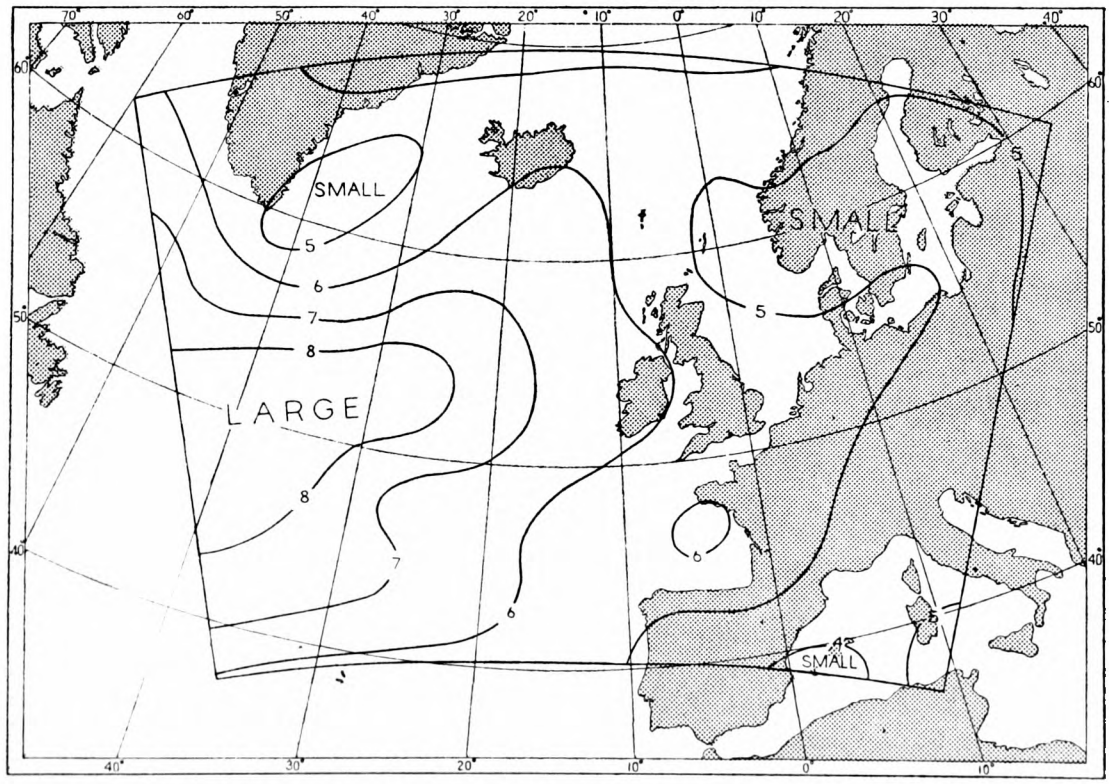

FIGURE 5(*f*). Root mean square 500–1000 mb thickness changes in tens of metres, 24-hour periods

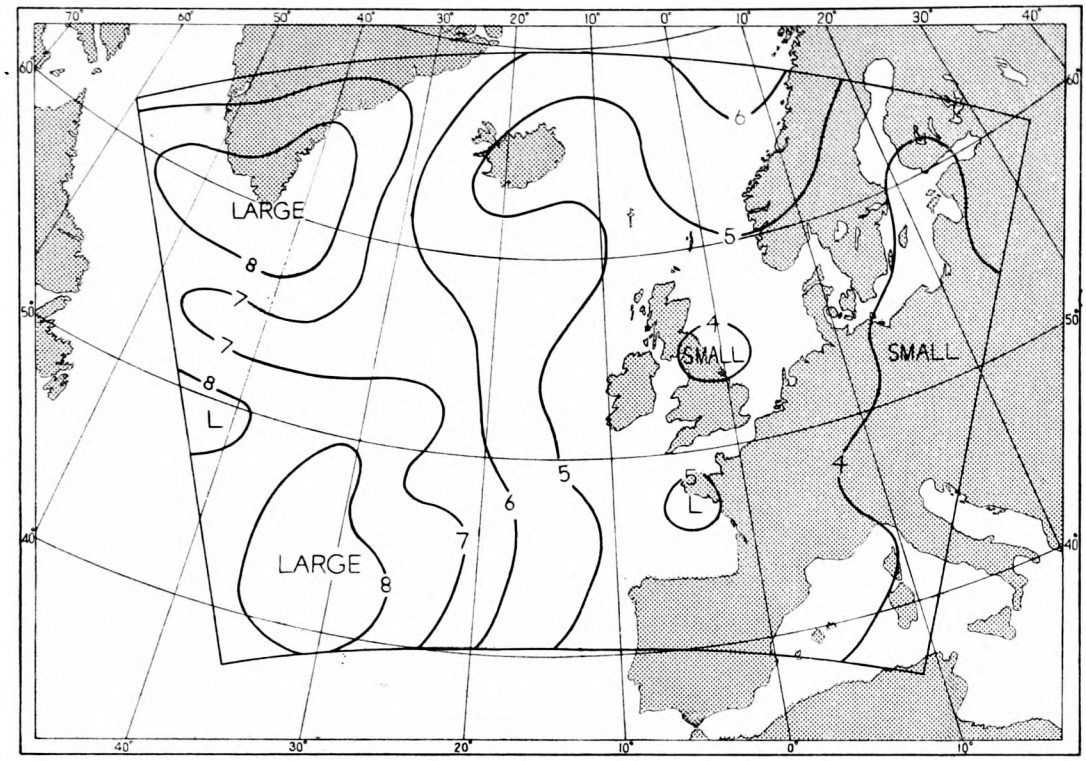

FIGURE 5(*g*). Root mean square 500 mb contour height errors in tens of metres, 24-hour numerical forecasts

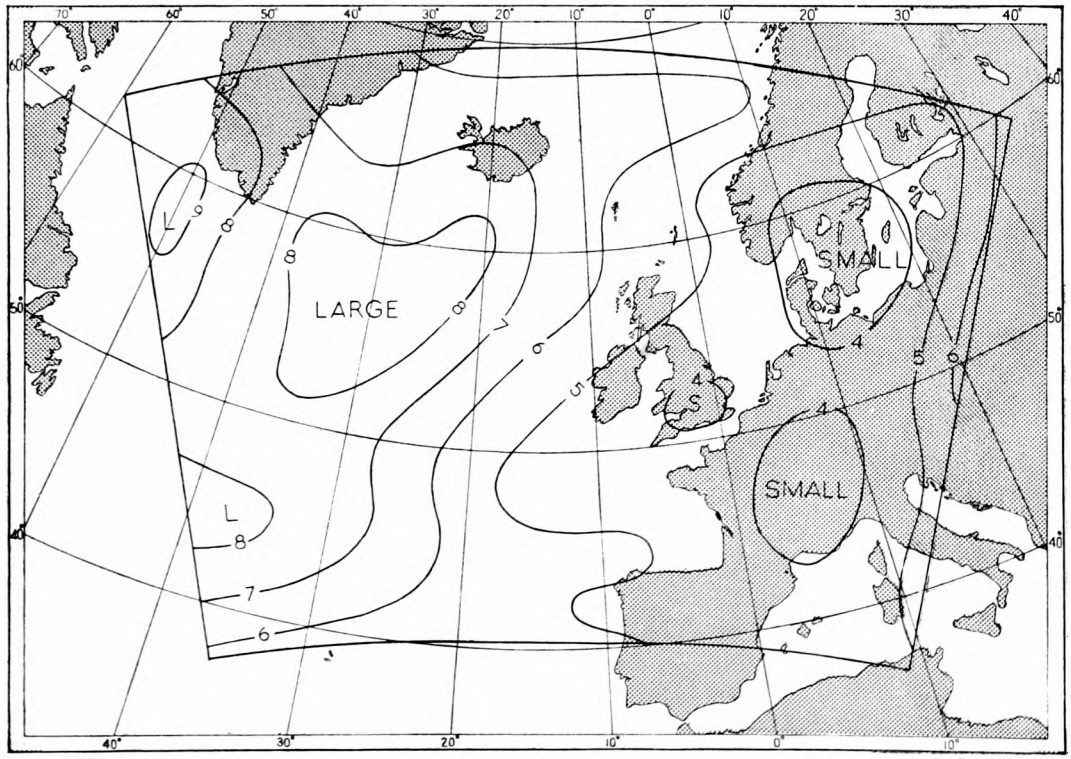

FIGURE 5(*h*). Root mean square 500 mb contour height errors in tens of metres, 24-hour C.F.O. forecasts

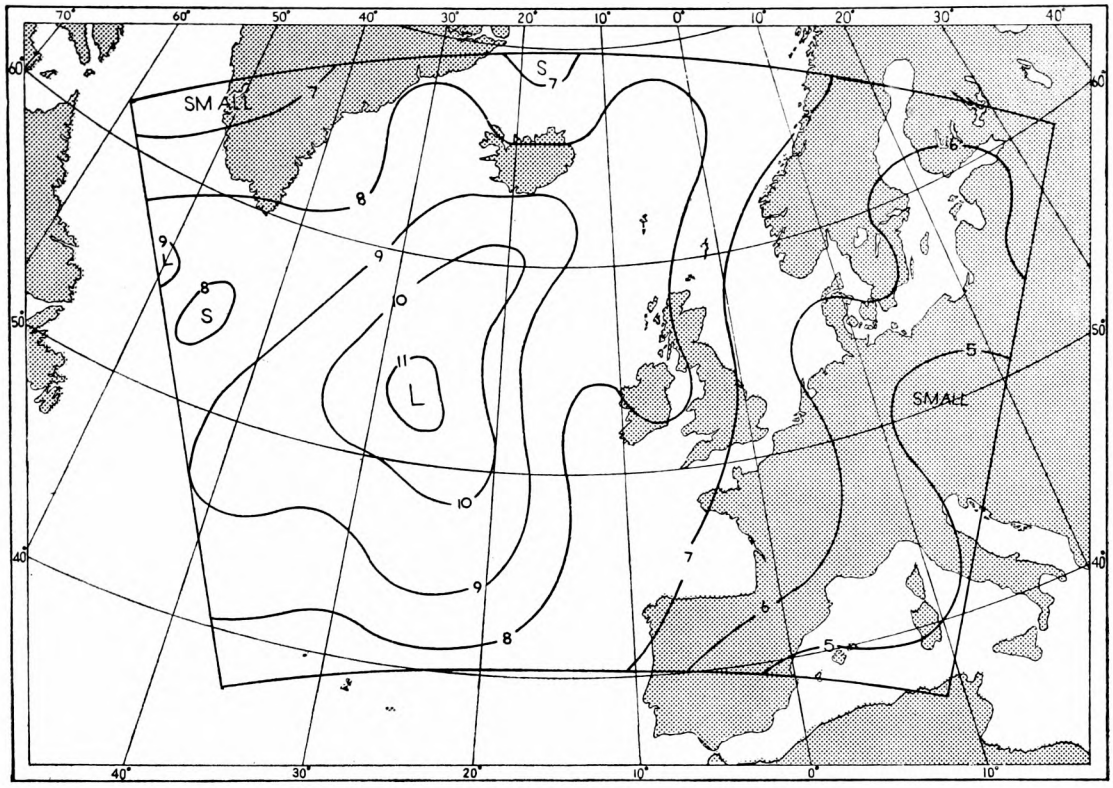

FIGURE 5(*i*). Root mean square 500 mb contour height changes in tens of metres, 24-hour periods

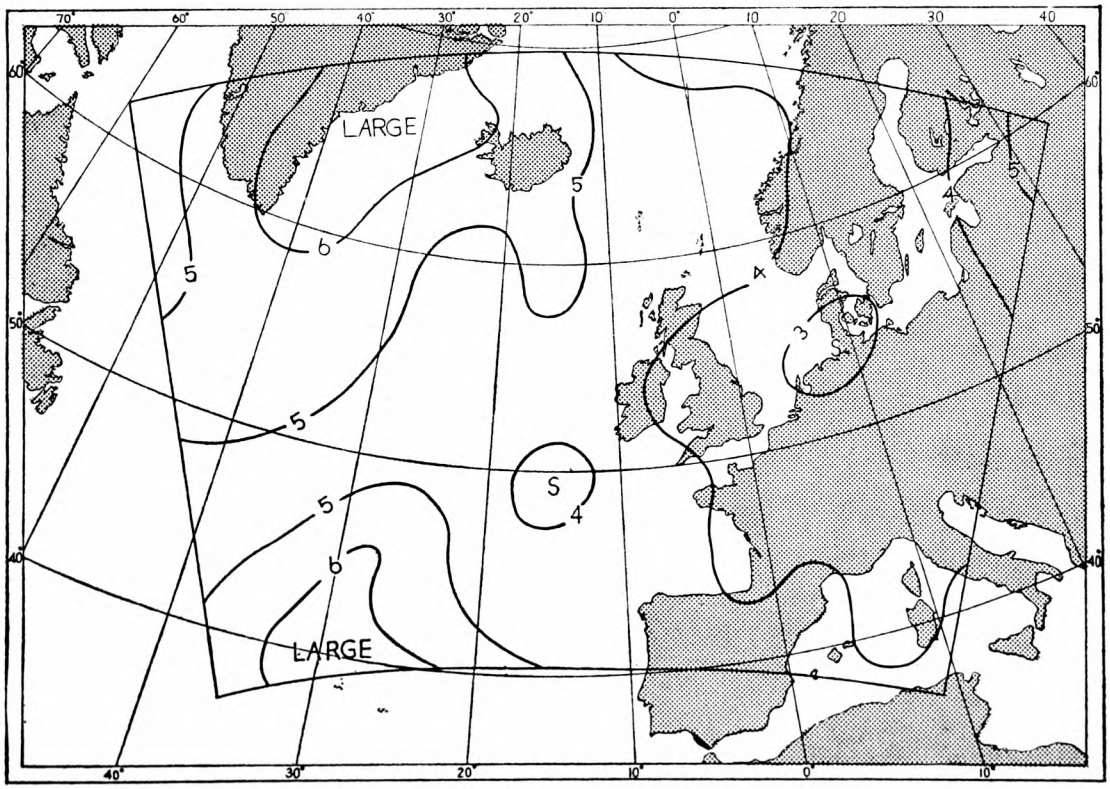

FIGURE 5(*j*). Root mean square 200–500 mb thickness errors in tens of metres, 24-hour numerical forecasts

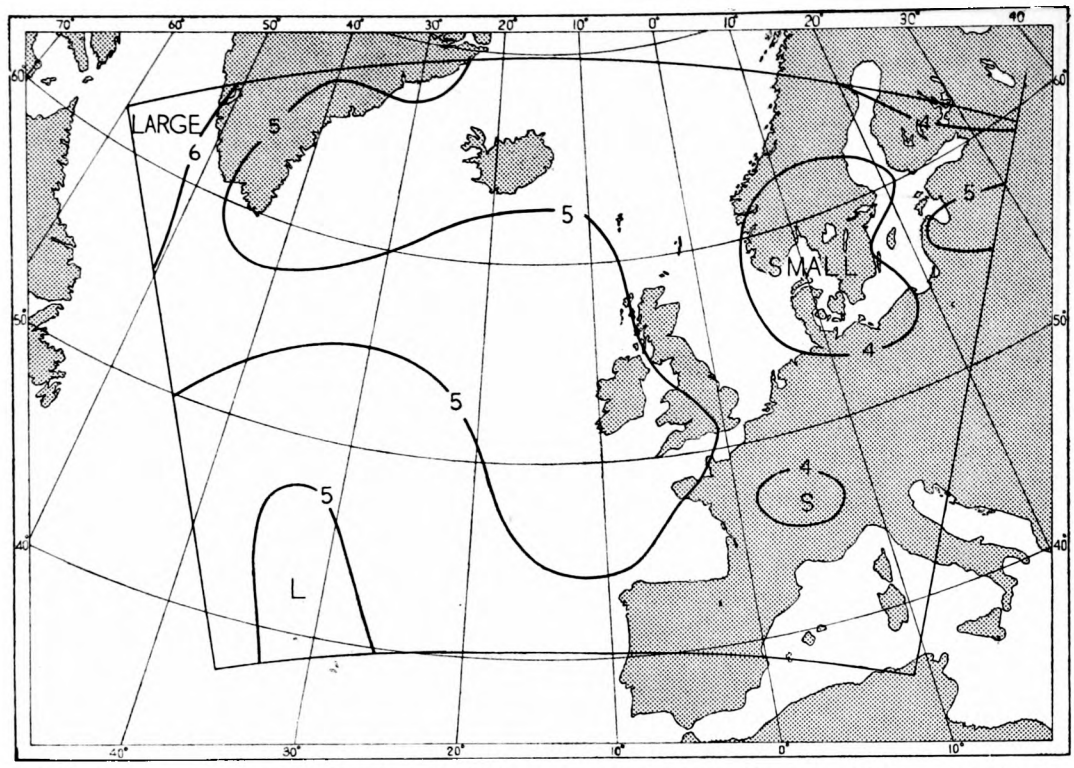

FIGURE 5(*k*). Root mean square 200–500 mb thickness errors in tens of metres, 24-hour C.F.O. forecasts

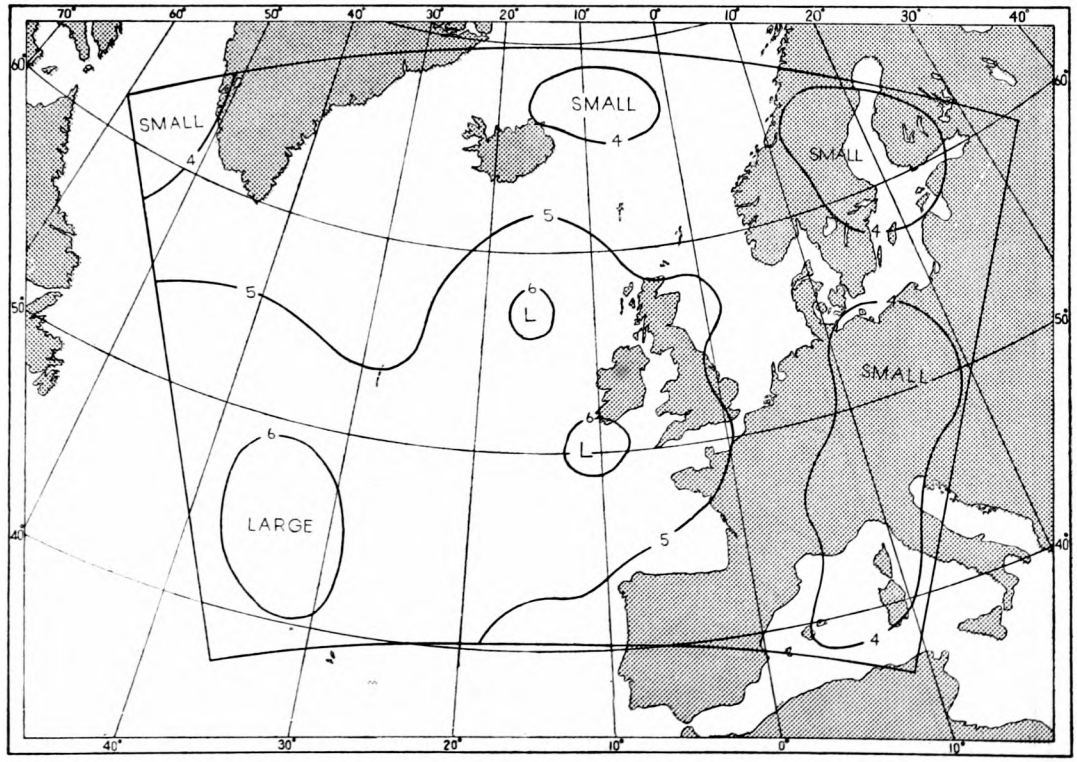

FIGURE 5(*l*). Root mean square 200–500 mb thickness changes in tens of metres, 24-hour periods

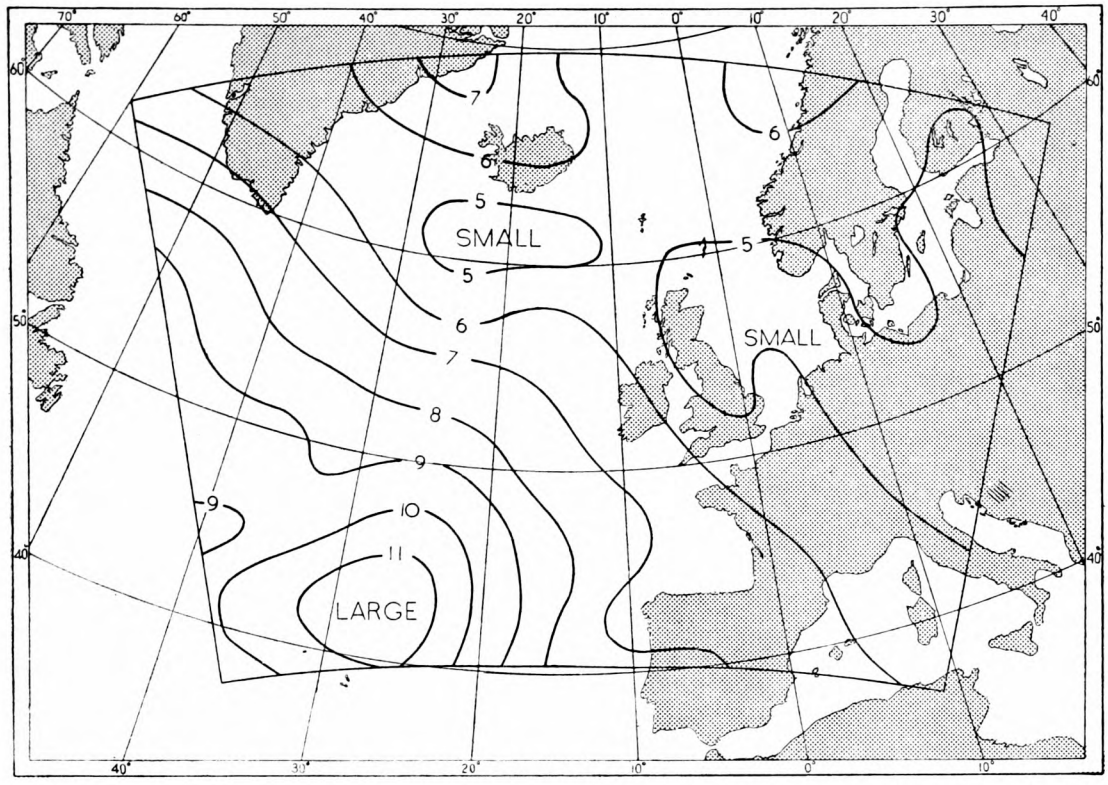

FIGURE 5(*m*). Root mean square 200 mb contour height errors in tens of metres, 24-hour numerical forecasts

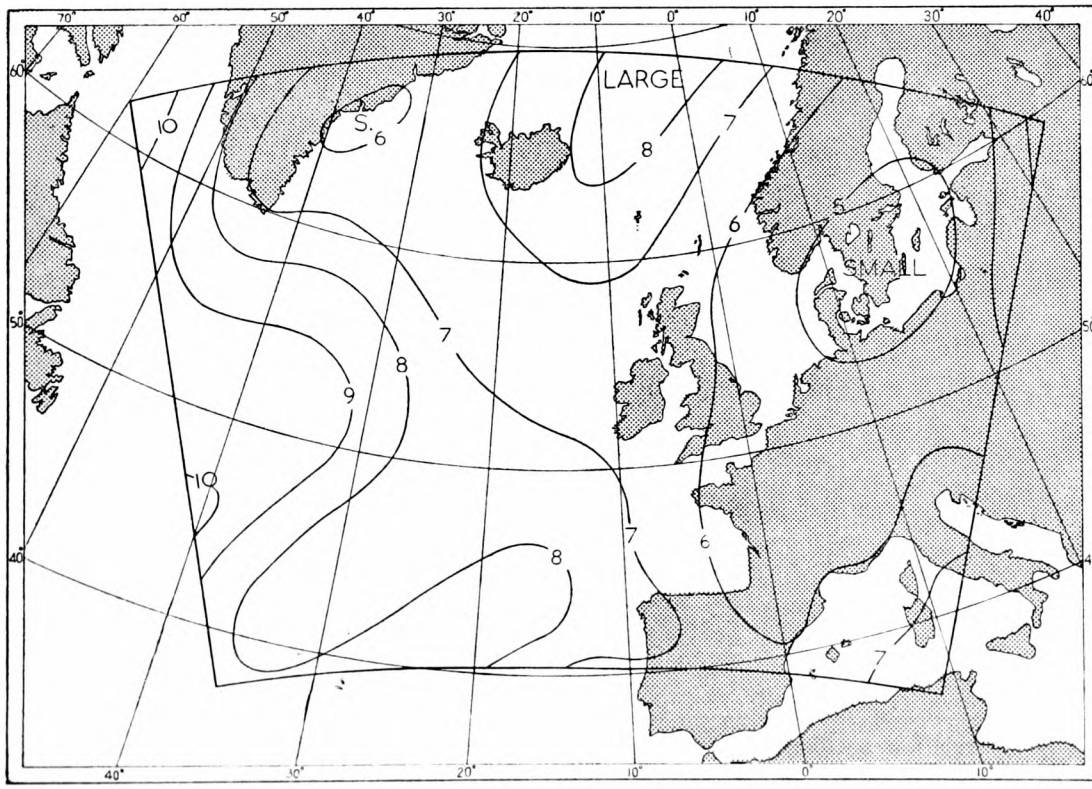

FIGURE 5(*n*). Root mean square 200 mb contour height errors in tens of metres, 24-hour C.F.O. forecasts

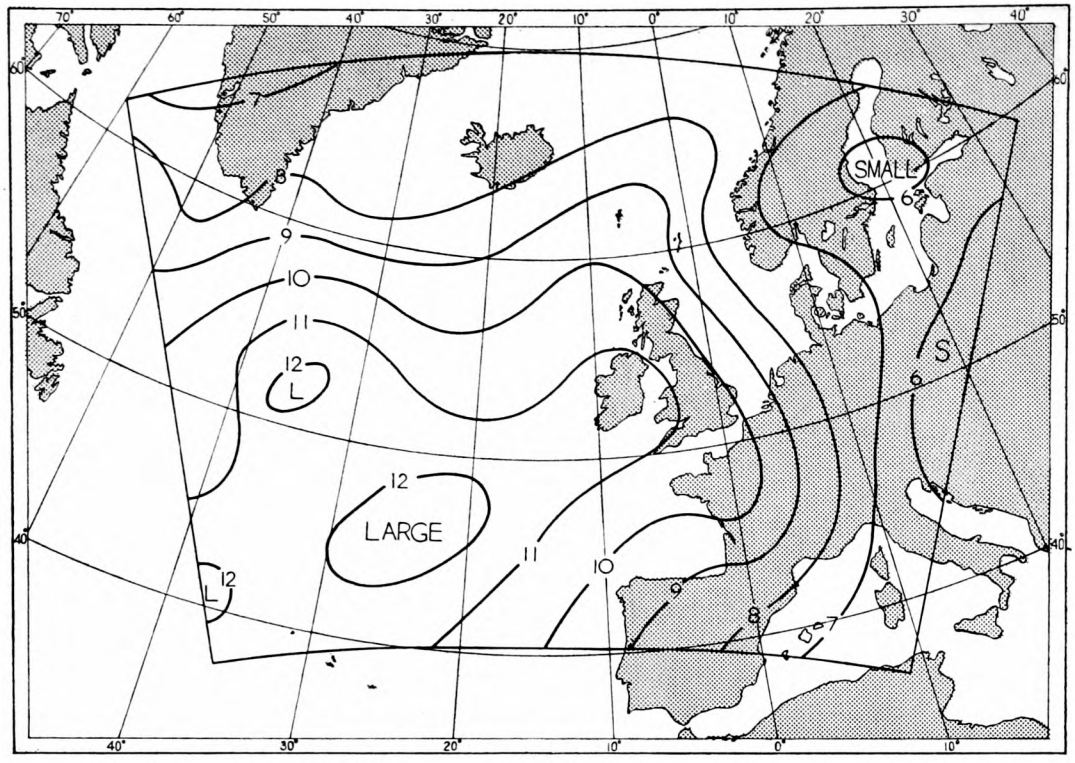

FIGURE 5(*o*). Root mean square 200 mb contour height changes in tens of metres, 24-hour periods

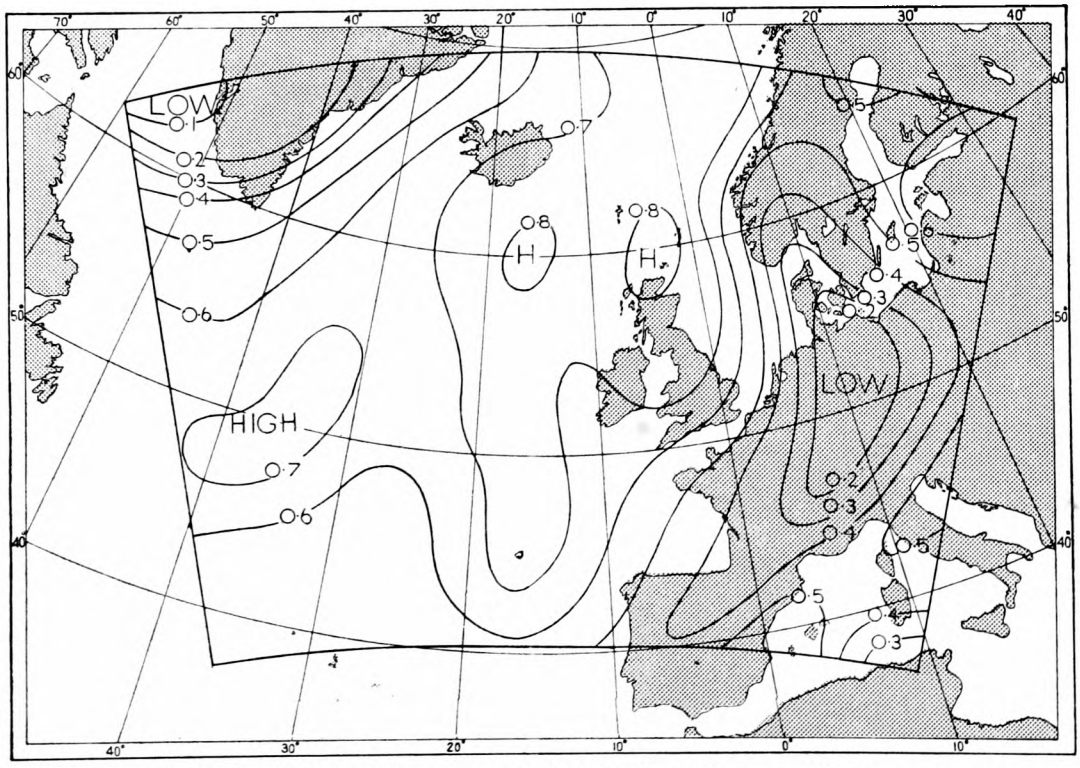

FIGURE 6(*a*). Correlation coefficients between numerical 24-hour forecast M.S.L. pressure changes and actual 24-hour pressure changes
55 cases in the period 29 Feb.–2 June 1960.

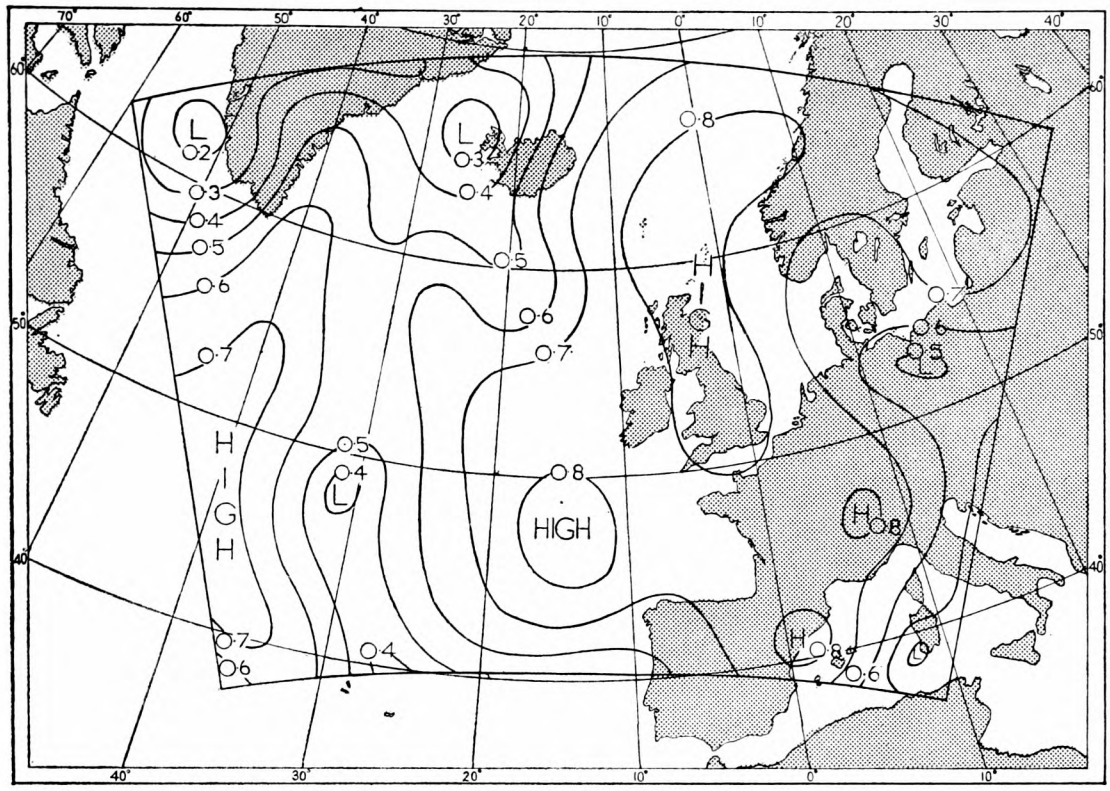

FIGURE 6(*b*). Correlation coefficients between C.F.O. 24-hour forecast M.S.L. pressure changes and actual 24-hour pressure changes

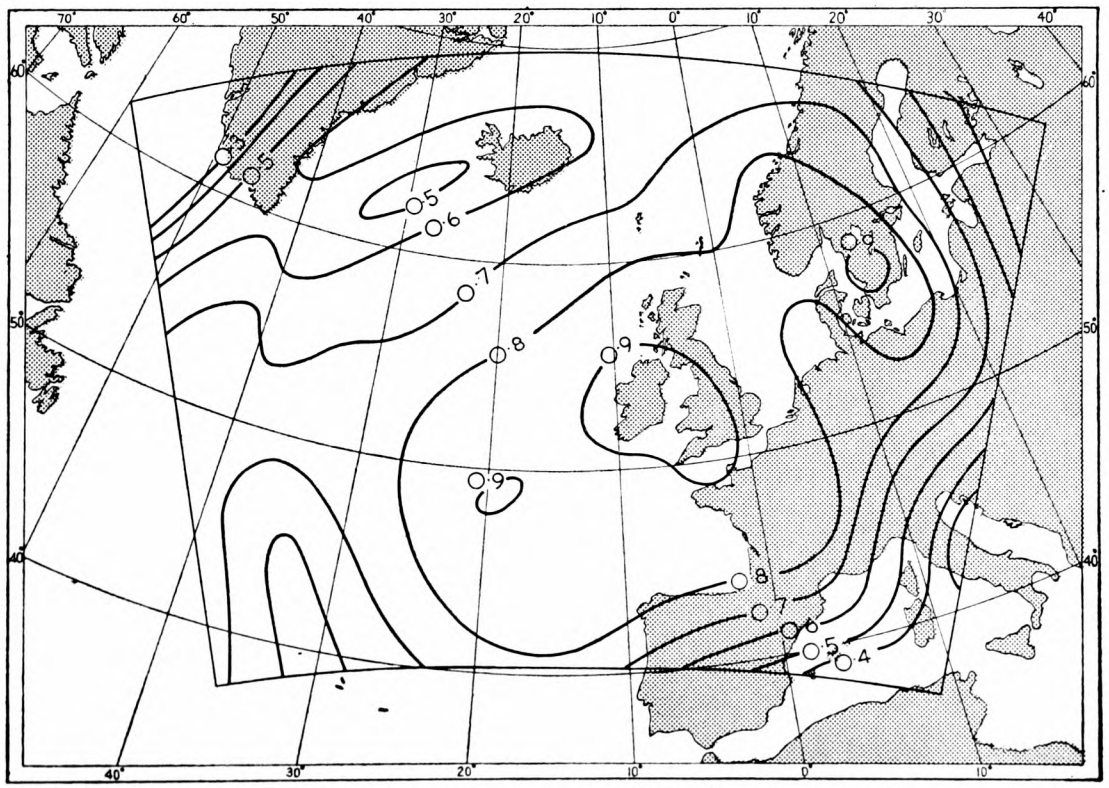

FIGURE 6(*c*). Correlation coefficients between numerical 24-hour forecast 500 mb contour height changes and actual 24-hour height changes

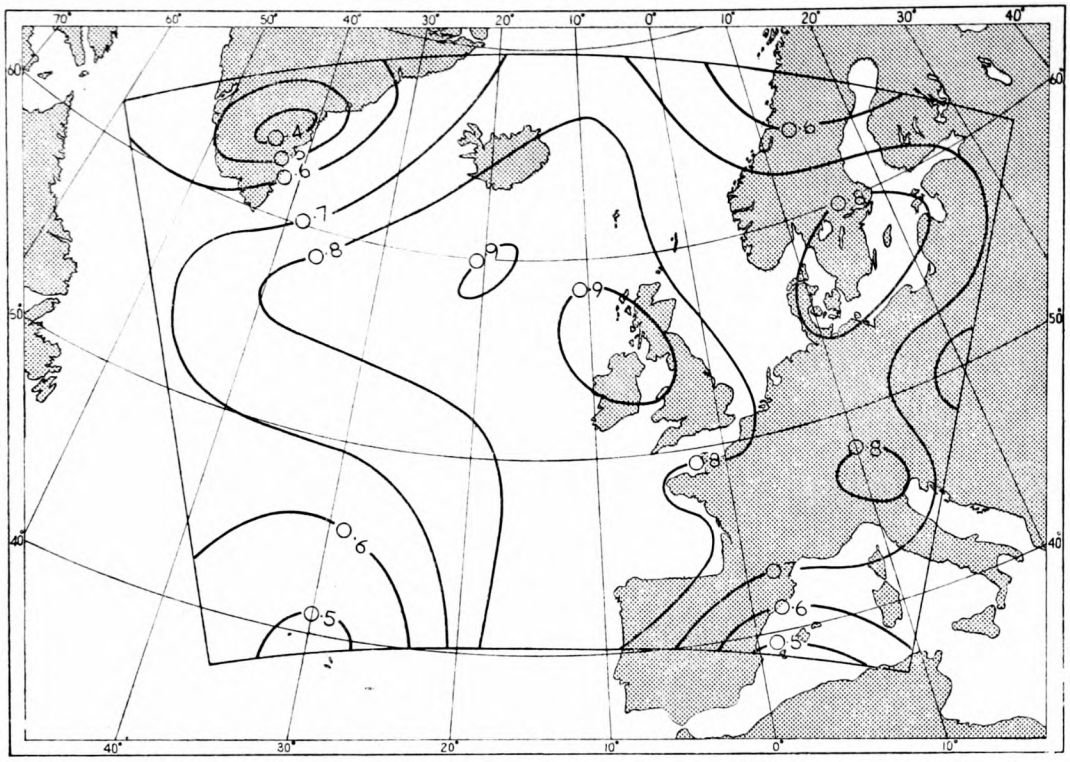

FIGURE 6(*d*). Correlation coefficients between C.F.O. 24-hour forecast 500 mb contour height changes and actual 24-hour height changes

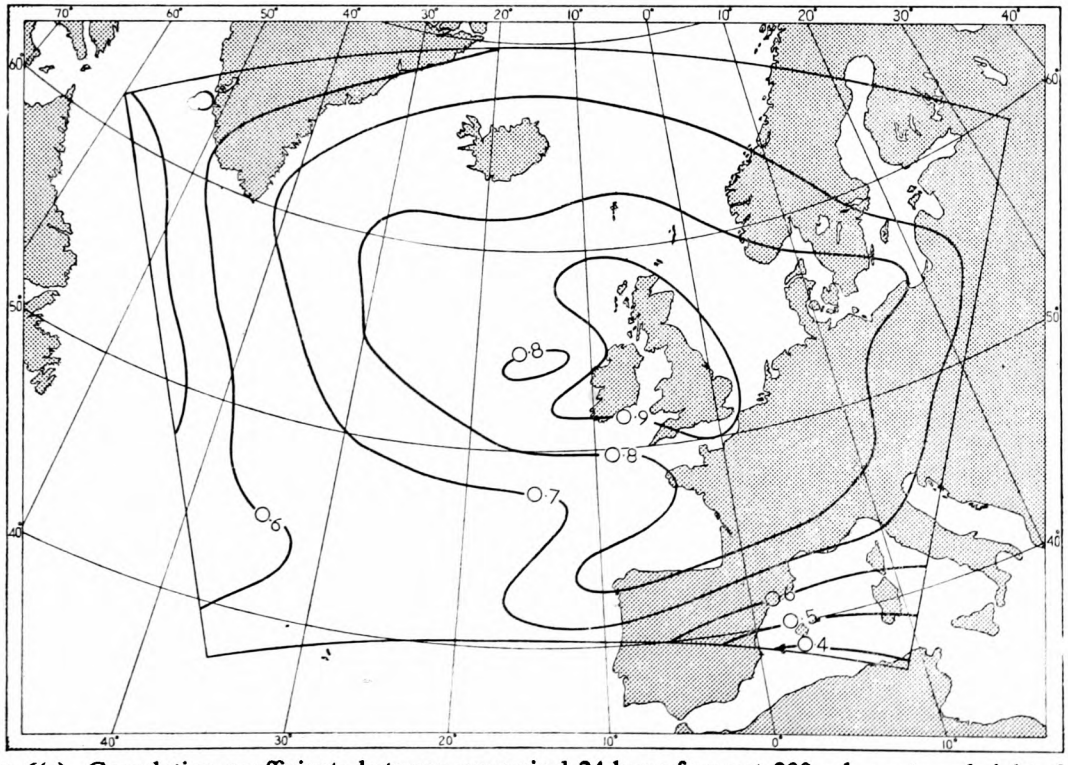

FIGURE 6(*e*). Correlation coefficients between numerical 24-hour forecast 200 mb contour height changes and actual 24-hour height changes

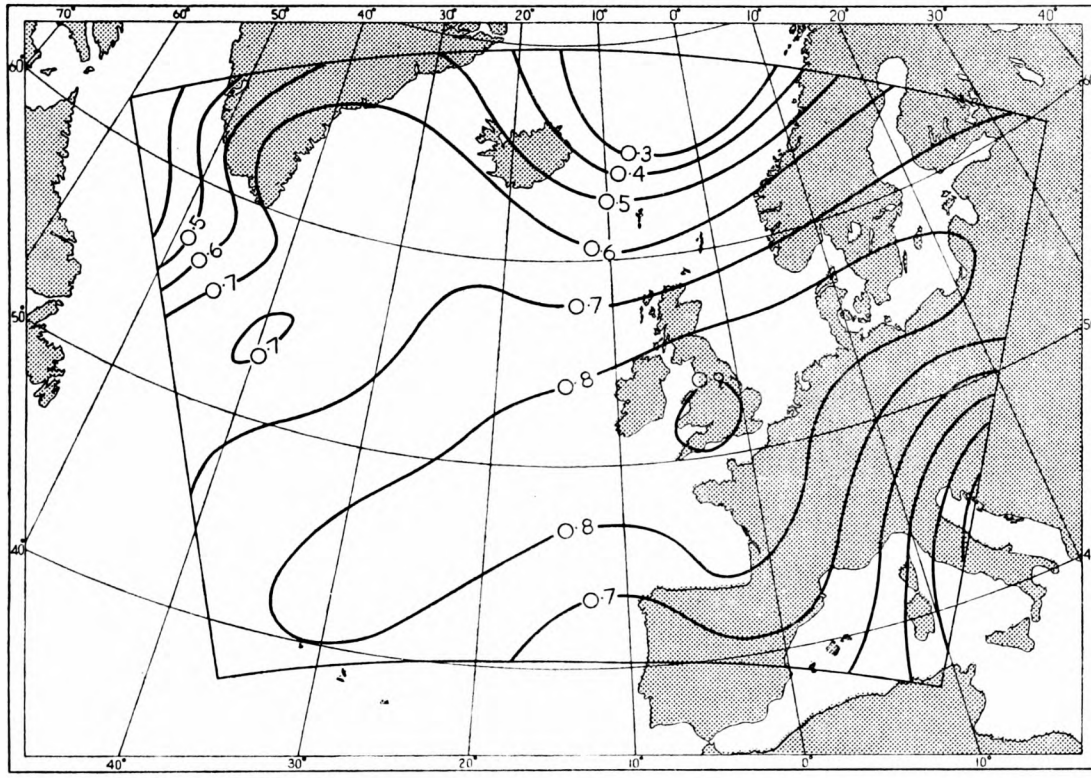

FIGURE 6(*f*). Correlation coefficients between C.F.O. 24-hour forecast 200 mb contour height changes and actual 24-hour height changes

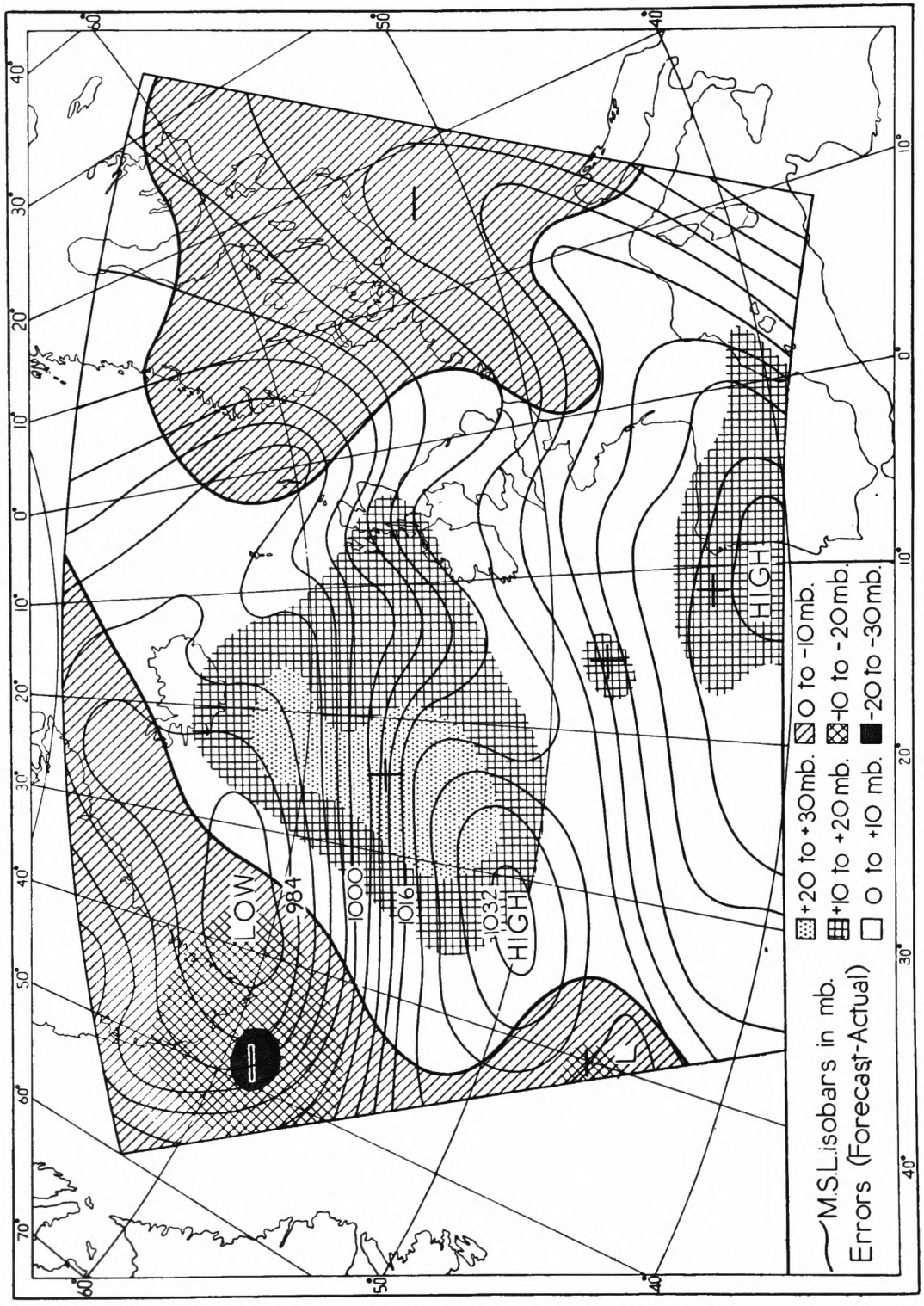

FIGURE 7(a). Numerical M.S.L. forecast and error field (forecast—actual pressure in millibars), 24-hour forecast for 0001 GMT, 13 April 1960

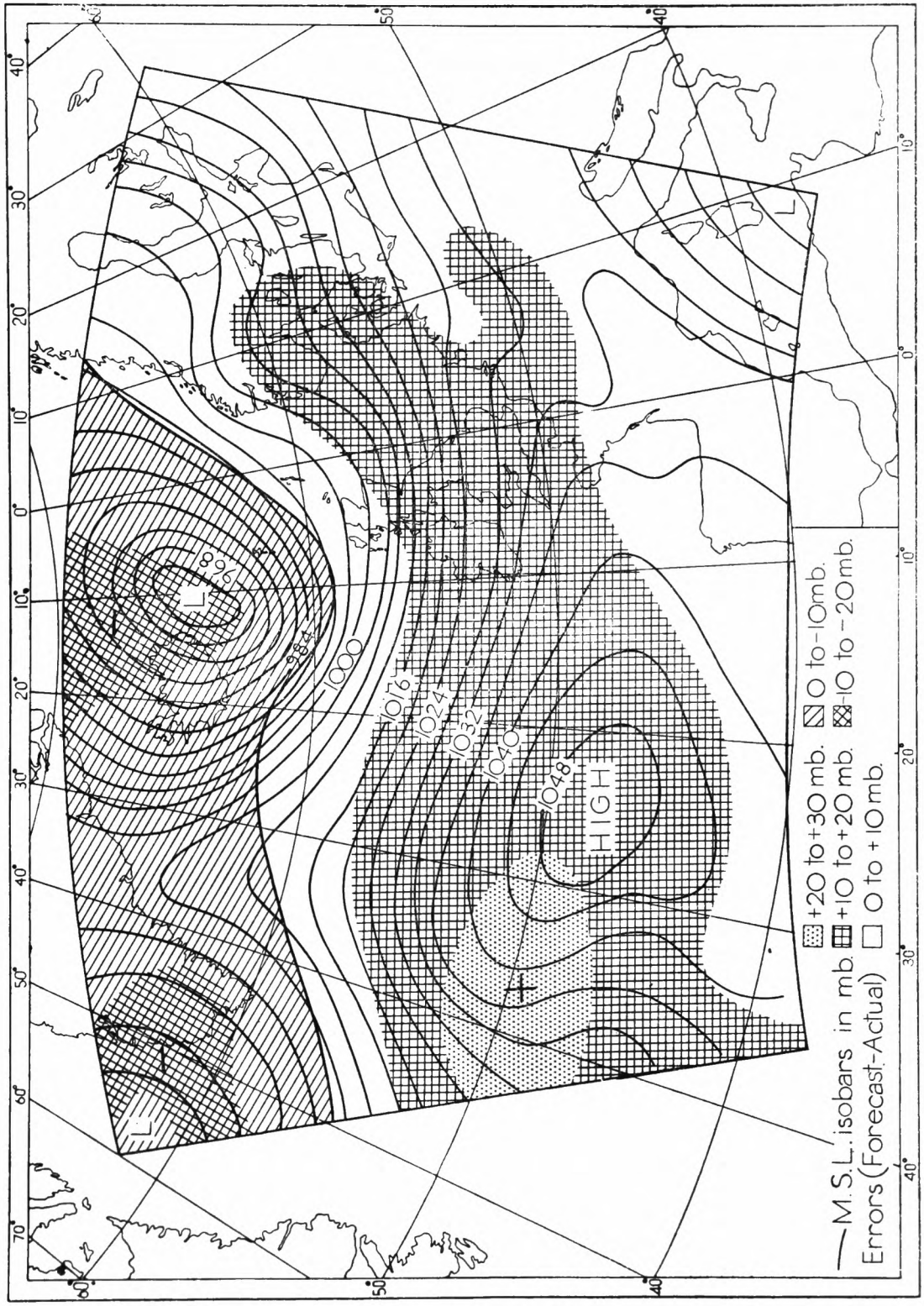

FIGURE 7(*b*). Numerical M.S.L. forecast and error field (forecast—actual pressure in millibars), 24-hour forecast for 0001 GMT, 14 April 1960

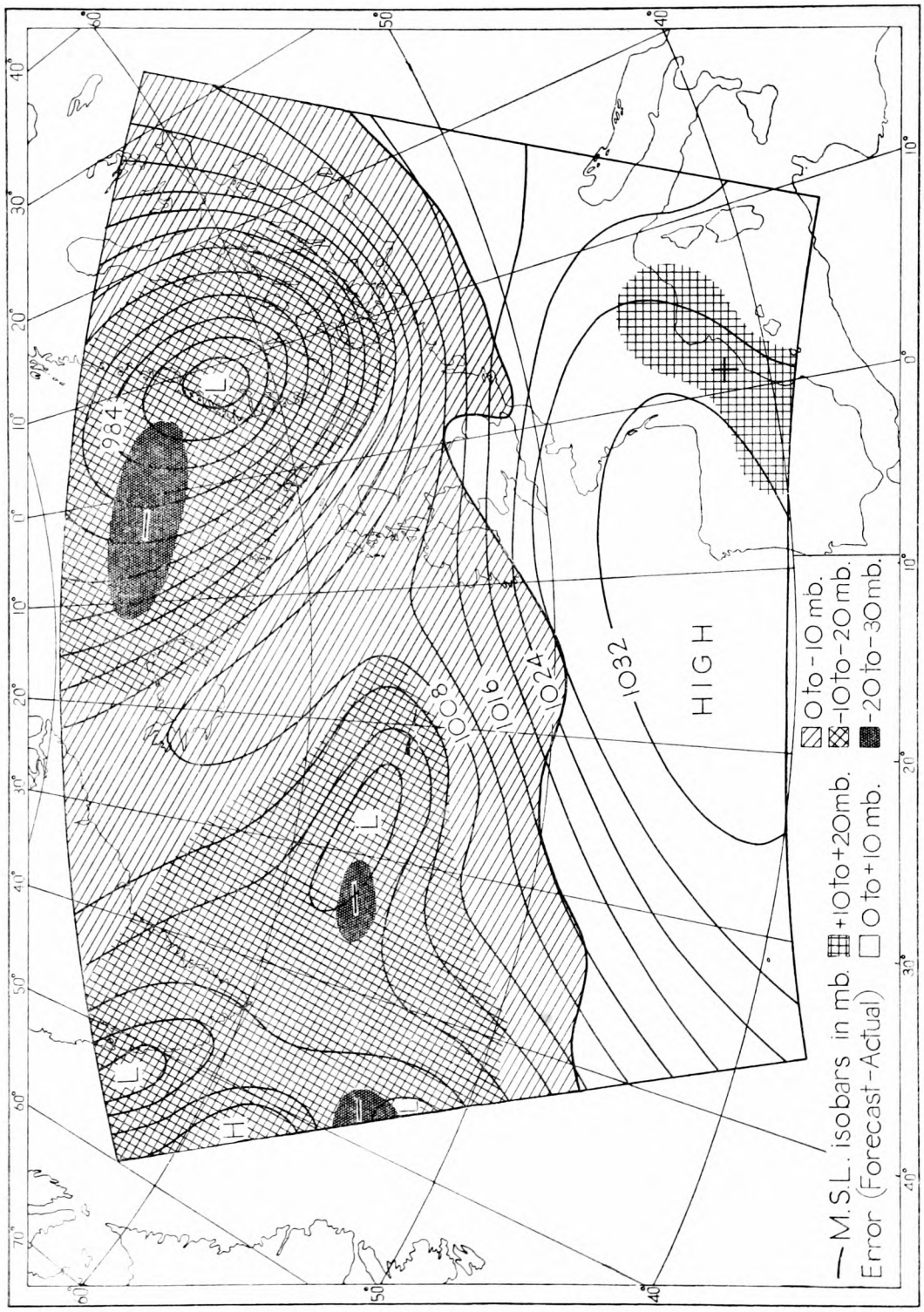

FIGURE 7(c). Numerical M.S.L. forecast and error field (forecast—actual pressure in millibars), 24-hour forecast for 0001 GMT, 15 April 1960

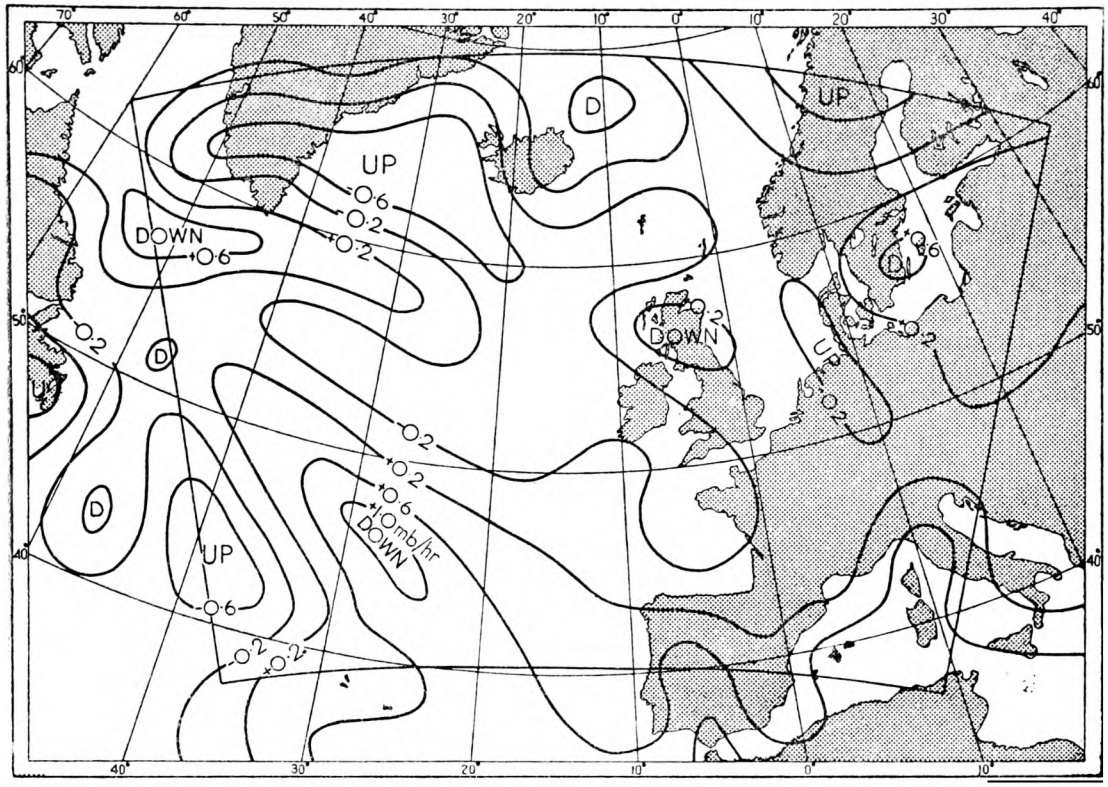

FIGURE 8(*a*). Average vertical motion field in the 1000–600 mb layer for 55 cases in the period 29 Feb.–2 June 1960. Mean vertical motion computed from the forecast contours and thicknesses

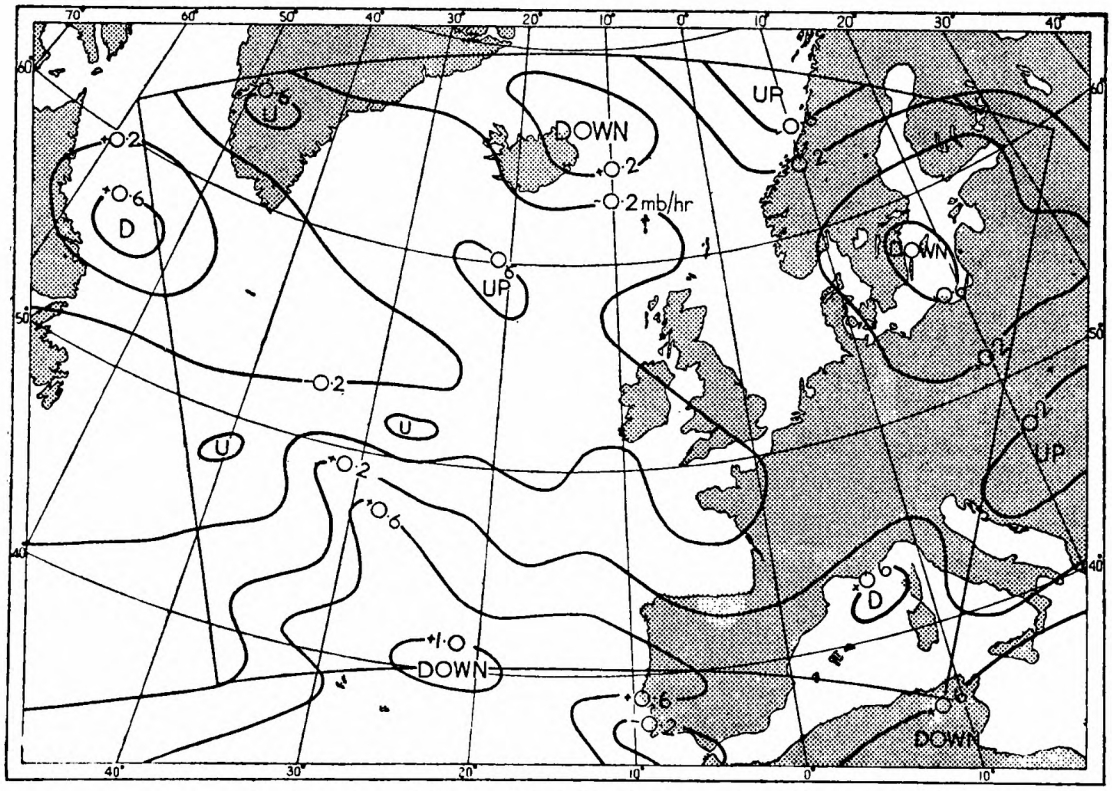

FIGURE 8(*b*). Average vertical motion field in 600–200 mb layer for 55 cases in the period 29 Feb.–2 June 1960. Mean vertical motion computed from the forecast contours and thicknesses

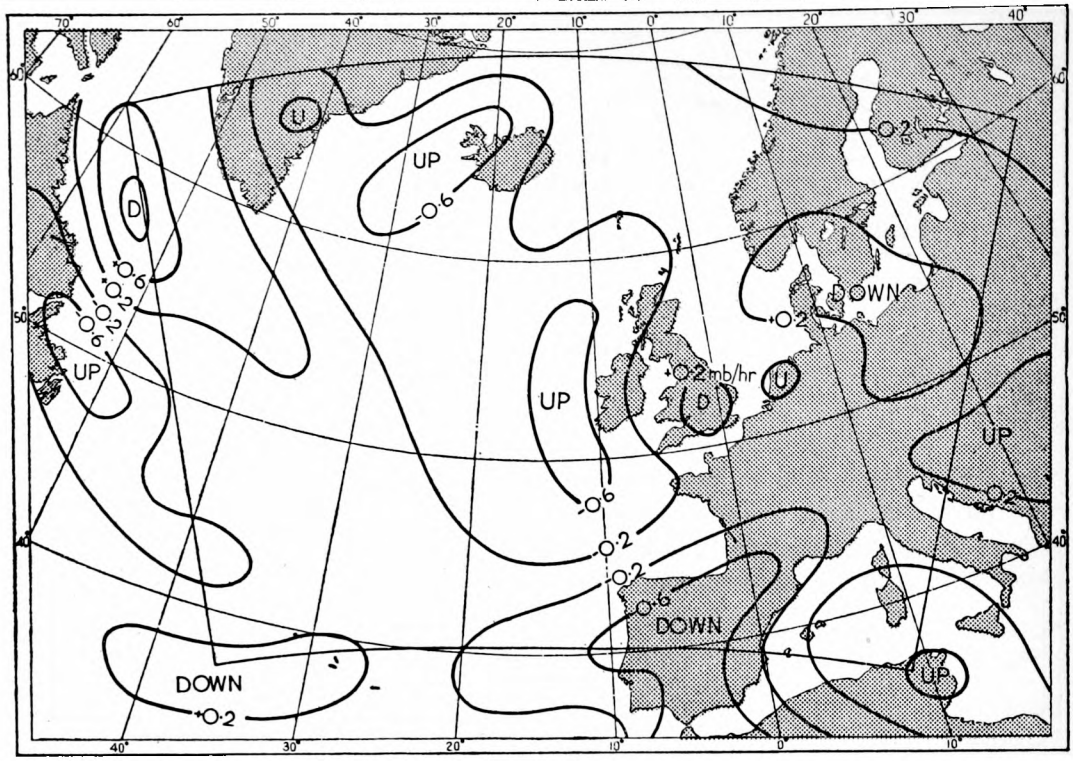

FIGURE 8(*c*). Average vertical motion field in the 1000–600 mb layer for 55 cases in the period 29 Feb.–2 June 1960. Mean vertical motion computed from the verifying contours and thicknesses

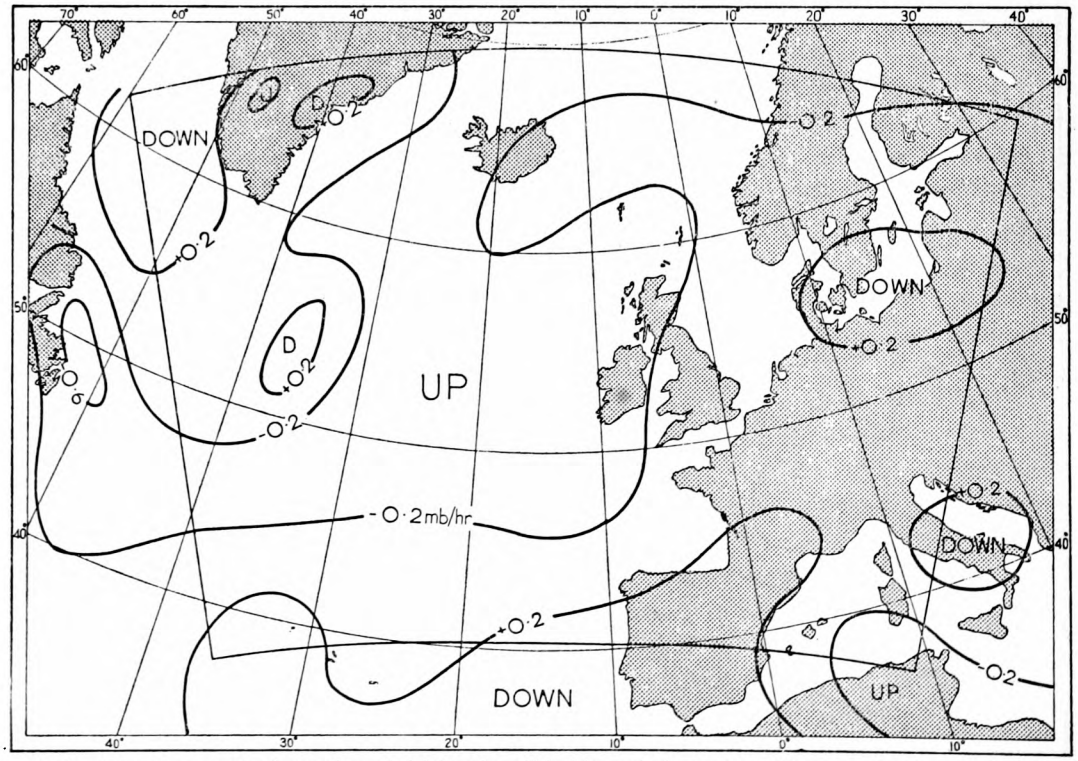

FIGURE 8(*d*). Average vertical motion field in the 600–200 mb layer for 55 cases in the period 29 Feb.–2 June 1960. Mean vertical motion computed from the verifying contours and thicknesses

Printed in England under the Authority of HER MAJESTY'S STATIONERY OFFICE by
James Townsend & Sons, Ltd., Exeter.

(B.11241) 106302 Wt.2179/BM.4185 K8 4/62 999/126

SCIENTIFIC PAPERS 4to.

1. Airborne measurements of the latitudinal variation of frost-point, temperature and wind; by N. C. Helliwell, B.Sc. M.O.664, 1960. 3*s*. 6*d*. (3*s*. 10*d*.).

2. Conservation of vorticity at 100 millibars; by J. R. Probert-Jones, B.A. M.O.673, 1960. 2*s*. 6*d*. (2*s*. 9*d*.).

3. The rainfall of Malta; by B. F. Bulmer, M.A., B.Sc. and K. Stormonth, B.Sc. M.O.676, 1960. 3*s*. 0*d*. (3*s*. 4*d*.).

4. Pressure variation over Malaya and the resonance theory; by R. Frost, B.A. M.O.678, 1960. 2*s*. 6*d*. (2*s*. 9*d*.).

5. An experiment in numerical forecasting; by E. Knighting, B.Sc., G. A. Corby, B.Sc., F. H. Bushby, B.Sc. and C. E. Wallington, M.Sc. M.O.682, 1961. 5*s*. (5*s*. 5*d*.).

6. Seasonal variation of the sea surface temperature in coastal waters of the British Isles; by F. E. Lumb, M.Sc. M.O.685, 1961. 3*s*. (3*s*. 4*d*.).

7. Forecasting in the Falkland Islands and Dependencies; by S. D. Glassey. M.O.687, 1961. 3*s*. 6*d*. (3*s*. 10*d*.).

8. Factors associated with the formation and persistence of anticyclones over Scandinavia in the winter half of the year; by M. K. Miles, M.Sc. M.O.692, 1961. 3*s*. (3*s*. 4*d*.).

9. An experiment in the verification of forecast charts; by C. E. Wallington, M.Sc. M.O.693, 1961. 4*s*. (4*s*. 4*d*.).

10. Incidence of, and some rules for forecasting, temperature inversions over the north-east Atlantic; by H. C. Shellard, B.Sc. and R. F. M. Hay, M.A. M.O.696, 1961. 3*s*. (3*s*. 4*d*.).

11. Some calculations of terms in the energy balance for monthly periods at the ocean weather stations I and J in the North Atlantic; by H. C. Shellard, B.Sc. M.O.712, 1962. 3*s*. (3*s*. 3*d*.).

12. Some statistical relationships between the temperature anomalies in neighbouring months in Europe and western Siberia; by J. M. Craddock, M.A. and R. Ward. M.O.718, 1962. (In the press).

Prices in brackets include postage.

Published by
HER MAJESTY'S STATIONERY OFFICE

To be purchased from
York House, Kingsway, London W.C.2
423 Oxford Street, London W.1
13A Castle Street, Edinburgh 2
109 St. Mary Street, Cardiff
39 King Street, Manchester 2
Tower Lane, Bristol 1
35 Smallbrook, Ringway, Birmingham 5
80 Chichester Street, Belfast
or through any bookseller

S.O. Code No. 40-164-13